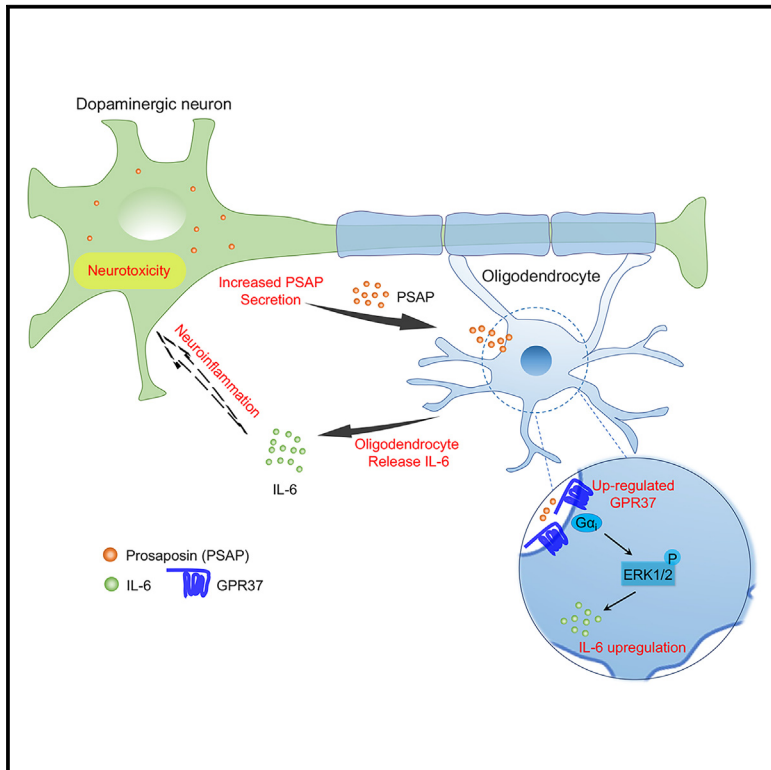


Oligodendrocytes drive neuroinflammation and neurodegeneration in Parkinson's disease via the prosaposin-GPR37-IL-6 axis

Graphical abstract



Authors

Qiang Ma, Jin-Lan Tian, Yao Lou, ..., Jing-Wei Zhao, Jing Zhang, Zhen-Zhong Xu

Correspondence

0618339@zju.edu.cn (Q.M.),
guoranxs@126.com (R.G.),
xuzz@zju.edu.cn (Z.-Z.X.)

In brief

Ma et al. identify that oligodendrocytes drive PD-like neurodegeneration via the prosaposin-GPR37-IL-6 axis. GPR37 is upregulated in oligodendrocytes, and prosaposin secretion is increased in parkinsonian mice. Released prosaposin could induce IL-6 upregulation and secretion from oligodendrocytes by GPR37 signaling, resulting in enhanced neuroinflammation, dopamine neuron degeneration, and behavioral deficits.

Highlights

- GPR37 is expressed in oligodendrocytes and upregulated in the substantia nigra of PD models
- GPR37 deficiency in oligodendrocytes rescues neurodegeneration in parkinsonian mice
- Prosaposin evokes upregulation of IL-6 in oligodendrocytes and PD-like dysfunction via GPR37
- IL-6 from oligodendrocytes is critical for the development of PD-like neurodegeneration



Article

Oligodendrocytes drive neuroinflammation and neurodegeneration in Parkinson's disease via the prosaposin-GPR37-IL-6 axis

Qiang Ma,^{1,2,3,9,*} Jin-Lan Tian,^{1,3,4,9} Yao Lou,^{2,9} Ran Guo,^{2,*} Xiao-Ru Ma,⁵ Jian-Bin Wu,⁵ Jing Yang,^{1,2} Bing-Jie Tang,^{1,3,4} Shun Li,² Mengsheng Qiu,⁶ Shumin Duan,^{1,3,4} Jing-Wei Zhao,⁵ Jing Zhang,^{1,3,7,8} and Zhen-Zhong Xu^{1,3,4,10,*}

¹Department of Anesthesiology of First Affiliated Hospital and School of Brain Science and Brain Medicine, Zhejiang University School of Medicine, Hangzhou 310058, China

²Center for Rehabilitation Medicine, Department of Anesthesiology and Department of Pain Management, Zhejiang Provincial People's Hospital, Affiliated People's Hospital, Hangzhou Medical College, Hangzhou 310014, China

³Liangzhu Laboratory, MOE Frontier Science Center for Brain Science and Brain-machine Integration, State Key Laboratory of Brain-machine Intelligence, Zhejiang University, Hangzhou 311121, China

⁴Nanhu Brain-Computer Interface Institute, NHC and CAMS Key Laboratory of Medical Neurobiology, Zhejiang University, Hangzhou 311100, China

⁵Department of Pathology of Sir Run Run Shaw Hospital and Department of Human Anatomy, Histology and Embryology, System Medicine Research Center, Zhejiang University School of Medicine, Hangzhou 310058, China

⁶Zhejiang Key Laboratory of Organ Development and Regeneration, Institute of Life Sciences, College of Life and Environmental Sciences, Hangzhou Normal University, Hangzhou 311121, China

⁷Department of Pathology of First Affiliated Hospital, Zhejiang University School of Medicine, Hangzhou 310002, China

⁸National Health and Disease Human Brain Tissue Resource Center, Zhejiang University, Hangzhou 310002, China

⁹These authors contributed equally

¹⁰Lead contact

*Correspondence: 0618339@zju.edu.cn (Q.M.), guoranxs@126.com (R.G.), xuzz@zju.edu.cn (Z.-Z.X.)

<https://doi.org/10.1016/j.celrep.2025.115266>

SUMMARY

Parkinson's disease (PD) is a common neurodegenerative disease and is difficult to treat due to its elusive mechanisms. Recent studies have identified a striking association between oligodendrocytes and PD progression, yet how oligodendrocytes regulate the pathogenesis of PD is still unknown. Here, we show that G-protein-coupled receptor 37 (GPR37) is upregulated in oligodendrocytes of the substantia nigra and that prosaposin (PSAP) secretion is increased in parkinsonian mice. The released PSAP can induce interleukin (IL)-6 upregulation and secretion from oligodendrocytes via a GPR37-dependent pathway, resulting in enhanced neuroinflammation, dopamine neuron degeneration, and behavioral deficits. GPR37 deficiency in oligodendrocytes prevents neurodegeneration in multiple PD models. Finally, the hallmarks of the PSAP-GPR37-IL-6 axis are observed in patients with PD. Thus, our results reveal that dopaminergic neurons interact with oligodendrocytes via secreted PSAP, and our findings identify the PSAP-GPR37-IL-6 axis as a driver of PD pathogenesis and a potential therapeutic target that might alleviate PD progression in patients.

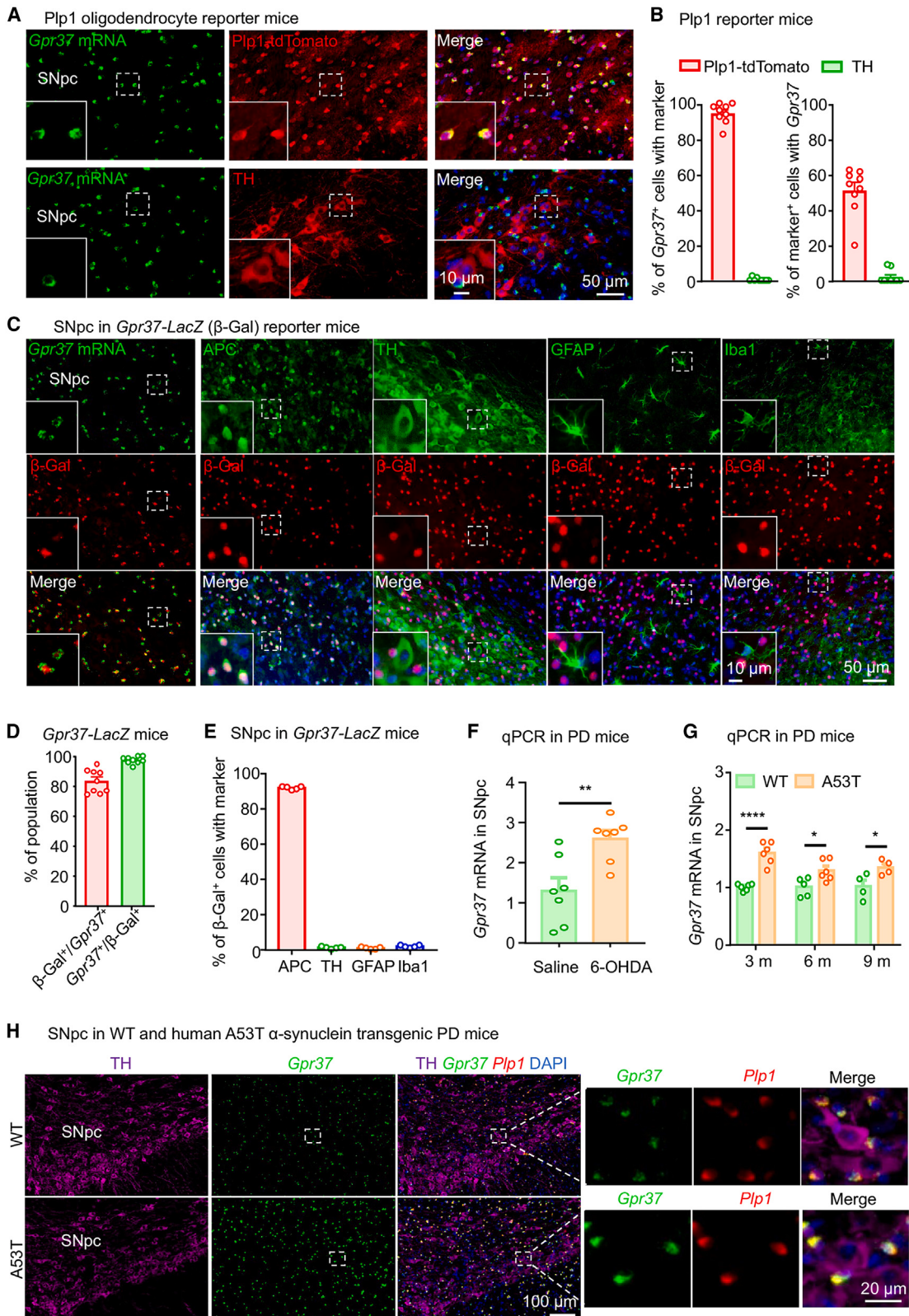
INTRODUCTION

Parkinson's disease (PD) is one of the most common neurodegenerative disorders and is characterized by the degeneration of dopaminergic (DA) neurons in the substantia nigra pars compacta (SNpc).¹ Pathologic DA depletion in the basal ganglia results in motor deficits of PD, such as rigidity, bradykinesia, and resting tremor.^{2,3} PD is also associated with nonmotor symptoms, such as sensory disturbances and depression.⁴ Pain is a frequent and distressing nonmotor symptom of PD, affecting 30%–85% of patients, and tends to worsen as the disease progresses.⁵ Currently, there are no therapies available to slow down or arrest the progression of PD due to its elusive mecha-

nisms,^{6,7} although targeting specific circuits can rescue motor and mood deficits in PD animal models.^{8,9}

There is emerging evidence that glial dysfunction contributes to PD pathogenesis and progression in a non-cell-autonomous fashion.^{10,11} Indeed, microglial activation and astrogliosis have been observed in the SNpc of patients with PD, which suggests that neuroinflammation is involved in the cascade of events leading to neuronal degeneration.¹² Oligodendrocytes, which have received limited attention, now might be recognized as glial cells involved in immune modulation, particularly during the initiation of immune processes.^{13,14} Recent studies have identified a striking association between oligodendrocytes and PD.^{15,16} However, the specific molecular mechanisms





(legend on next page)

underlying the role of oligodendrocytes in PD pathogenesis remain poorly understood.

G-protein-coupled receptor 37 (GPR37), also known as parkin-associated endothelin-like receptor, was observed primarily in nigral DA neurons, and its abnormal accumulation contributed to neurotoxic progresses.^{17,18} However, whether GPR37 is expressed in DA neurons remains controversial.^{19,20} Interestingly, our preliminary results showed that GPR37 was specifically expressed in oligodendrocytes in the SNpc of patients with PD, based on the re-analysis of a single-nucleus RNA sequencing (snRNA-seq) dataset²¹ of postmortem SNpc from patients. Thus, we set out to investigate whether and how GPR37 in oligodendrocytes contributes to the development of PD.

In this study, we identified that GPR37 in oligodendrocytes controls PD pathogenesis by mediating interleukin (IL)-6 secretion into cerebrospinal fluid (CSF). We found that GPR37 is selectively expressed in oligodendrocytes but not DA neurons, while prosaposin (PSAP), an endogenous ligand of GPR37,²² is enriched in DA neurons. We discovered that increased secretion of PSAP in the CSF induces IL-6 upregulation in oligodendrocytes via GPR37, resulting in enhanced IL-6 secretion, neuroinflammation, and DA neuron degeneration. We further revealed that abolishing GPR37 in oligodendrocytes prevents the degeneration of DA neurons and behavioral impairment in multiple mouse models of PD. Importantly, the enriched expression of PSAP in human DA neurons and increased secretion of PSAP and IL-6 in the CSF were confirmed in patients with PD. Thus, our data indicate that targeting the PSAP-GPR37-IL-6 axis could be a promising therapeutic strategy for treating PD.

RESULTS

GPR37 is specifically expressed in oligodendrocytes and significantly upregulated in the SNpc of PD models

To confirm the expression pattern of GPR37 in the SNpc, we first used *in situ* hybridization to probe *Gpr37* mRNA in the *Pip1-Cre/ER;Ai14* oligodendrocyte reporter mouse SNpc. Different from a previous report,¹⁸ we found a unique distribution pattern in which *Gpr37* was specifically expressed in *tdTomato*⁺ oligodendrocytes but not tyrosine hydroxylase (TH; a DA neuron marker)-positive DA neurons (Figures 1A and 1B). We also used the *Gpr37-LacZ* reporter mouse, which contains a bacterial β-galactosidase (β-gal) reporter gene in the *Gpr37* locus,^{19,20,23} to determine *Gpr37* mRNA expression in the SNpc (Figures 1C and 1D). We found that *Gpr37*-expressing nuclei (labeled by β-gal) were primarily observed in adenomatous polyposis coli (APC)⁺ oligodendrocytes,²⁴ and we did not find colocalization of β-gal-

labeled nuclei with TH, Iba1 (a marker for microglia), or GFAP (a marker for astrocytes) (Figures 1C–1E).

To determine the potential role of GPR37 in PD development, we evaluated the expression of *Gpr37* mRNA in 6-hydroxydopamine (6-OHDA) intoxication-induced PD mouse, human A53T alpha-synuclein (hA53T-αSyn; which plays a critical role in PD pathogenesis^{6,10,25–27}) transgenic PD mouse, and adeno-associated viral-mediated hA53T-αSyn (AAV-αSyn) overexpression PD mouse SNpcs. As shown in Figure 1F, *Gpr37* mRNA was significantly augmented in the SNpc 1 week after 6-OHDA injection. Similarly, *Gpr37* mRNA was also upregulated, especially at the early stage of A53T transgenic mice (Figure 1G) and AAV-αSyn-injected PD mice (Figure S1A). Furthermore, *Gpr37* mRNA was still confined to *Pip1*⁺ oligodendrocytes in the SNpc of hA53T transgenic mice (Figure 1H) and AAV-αSyn-injected PD mice (Figure S1B).

These results indicate that GPR37 is selectively expressed in oligodendrocytes and significantly upregulated in the SNpc of PD models.

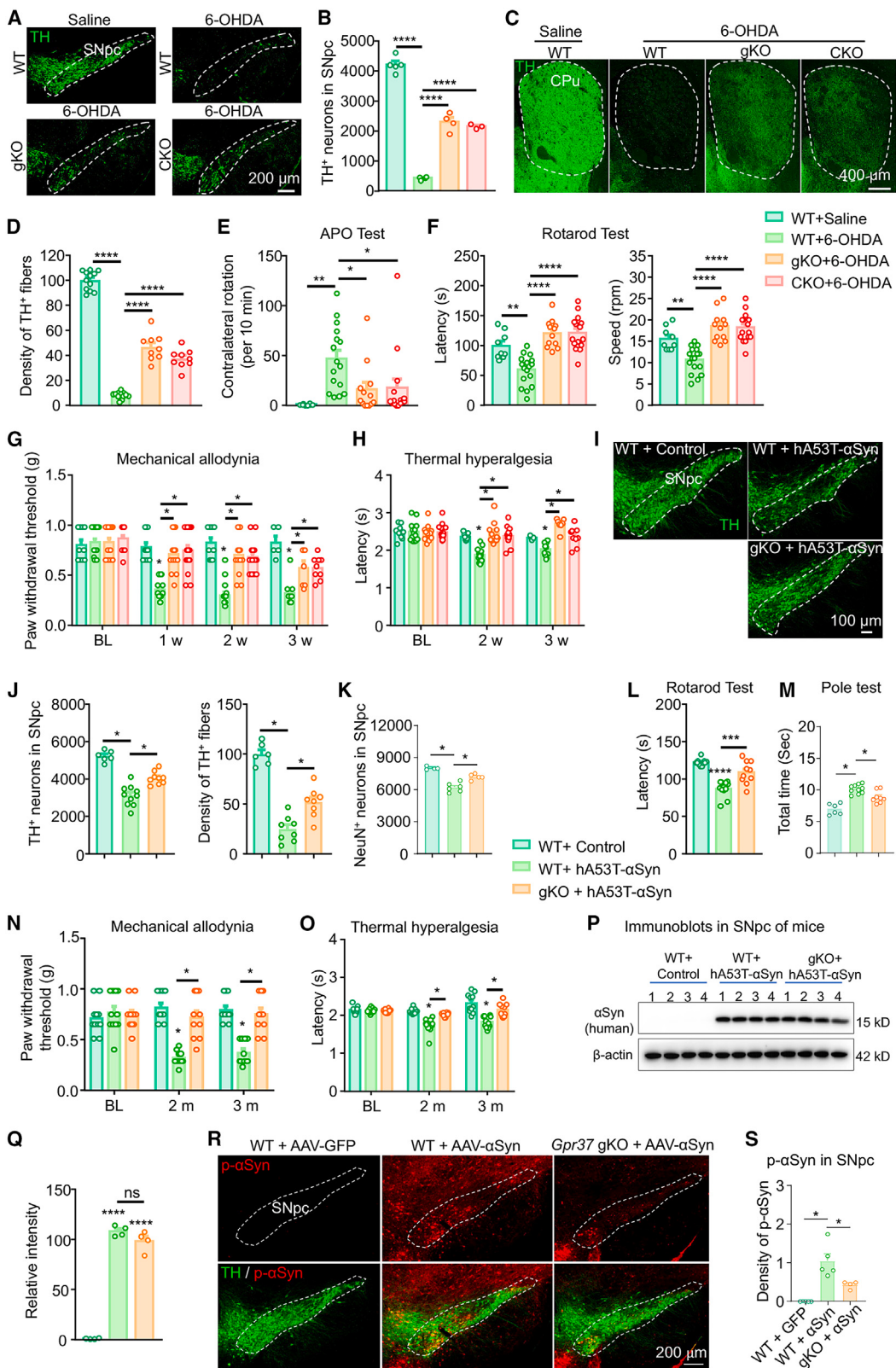
GPR37 deficiency in oligodendrocytes attenuates 6-OHDA- or hA53T-αSyn-induced neurodegeneration and behavioral deficits

To characterize the function of GPR37 in oligodendrocytes, we generated the *Gpr37* conditional knockout (CKO) mice (Figures S2A and S2B). We showed that *Gpr37* CKO mice displayed no deficits in motor function (Figures S2C and S2D) or basal pain threshold (Figures S2E and S2F). To detect the possible changes of myelin and associated axons in *Gpr37* CKO mice, we assessed the integrity of myelin and associated axons by transmission electron microscopy (EM). EM data showed that the axon's diameter (Figures S2G–S2J), myelin G-ratio (Figures S2K–S2N), and number of myelinated axons (Figures S2O and S2P) in the corpus callosum (CC) and striatum (caudate putamen [CPu]) were not significantly different between wild-type (WT) and *Gpr37* CKO mice. These data indicate that CKO of *Gpr37* in oligodendrocytes does not impair the integrity of myelin sheath and associated axons, overall functions, or basal pain in mice.

To assess whether GPR37 within oligodendrocytes is essential for intoxication-triggered loss of DA neurons, 6-OHDA was unilaterally injected into the medial forebrain bundle (MFB) of WT, *Gpr37* global KO (gKO), and *Gpr37* CKO mice. DA neuron loss was significantly attenuated in 6-OHDA-injected *Gpr37* gKO and CKO mice when compared to WT mice (Figures 2A and 2B). *Gpr37* gKO and CKO mice exhibited a corresponding, significant rescue of density in the ipsilateral striatum

Figure 1. GPR37 is specifically expressed in oligodendrocytes and significantly upregulated in the SNpc of PD models

- (A) Colocalization of *Gpr37* mRNA with *tdTomato* and TH in SNpc of *Pip1-Cre/ER;Ai14* mice. Scale bar: 50 μm. Insets represent the corresponding zoomed areas. Scale bar: 10 μm.
 - (B) Percentage quantification of *Gpr37*⁺ cells colocalized with *tdTomato* or TH ($n = 9$).
 - (C) Colocalization of β-gal with *Gpr37* mRNA, APC, TH, GFAP, and Iba1 in SNpc of *Gpr37-LacZ* reporter mouse. Scale bars: 50 and 10 μm (insets).
 - (D) Quantification of *Gpr37*⁺ cells colocalized with β-gal in SNpc ($n = 9$).
 - (E) Percentage of β-gal⁺ cells coexpressing each marker ($n = 5$ /group).
 - (F and G) The upregulation of *Gpr37* mRNA in SNpc from 6-OHDA-induced PD mice (F) or human A53T α-synuclein transgenic mice (G). $n = 4$ –7.
 - (H) Colocalization of *Gpr37* mRNA with *Pip1* mRNA and TH in SNpc of WT or A53T transgenic mice (6 months). Scale bars: 100 μm and 20 μm.
- All data are means ± SEM. * $p < 0.05$, ** $p < 0.01$, and *** $p < 0.0001$ by two-tailed Student's unpaired t test (F) and Bonferroni's two-way ANOVA (G).



(legend on next page)

(Figures 2C and 2D). Additionally, we found that GPR37 deficiency significantly prevented 6-OHDA-induced motor deficits as determined by the apomorphine (APO)-induced rotation test^{28,29} and rotarod test (Figures 2E and 2F). Pain is a prevalent and increasingly recognized nonmotor symptom of PD, affecting 30%–85% of the patient population.^{5,30} As shown in Figures 2G and 2H, 6-OHDA triggered mechanical and thermal hypersensitivity in WT mice as previously reported,³¹ and both mechanical (Figure 2G) and thermal (Figure 2H) pain were relieved in 6-OHDA-injected *Gpr37* gKO and CKO mice.

To better understand the role of GPR37 in patients suffering from PD, we constructed an AAV-mediated hA53T- α Syn overexpression mouse PD model, which reflected the clinical and pathological hallmarks of human PD.³² As previously described, unilateral AAV- α Syn injection led to a decrease in nigral DA neurons and ipsilateral striatal TH⁺ optical density (Figures 2I–2K). In contrast, mice lacking *Gpr37* were resistant to AAV- α Syn-induced neurodegeneration (Figures 2I–2K). Furthermore, AAV- α Syn induced motor impairment (Figures 2L and 2M) as well as chronic mechanical and thermal pain (Figures 2N and 2O) in WT mice but not in *Gpr37* gKO mice (Figures 2L–2O). The expression of total α Syn was equivalent in WT and gKO mice (Figures 2P and 2Q). To determine whether GPR37 regulates the formation of pathologic α Syn, we examined the phosphorylated α Syn Ser129 (p- α Syn), which is considered the typical pathological form of α Syn.^{33,34} Notably, AAV- α Syn treatment induced a robust increase of p- α Syn accumulations in the SNpc of WT mice, while p- α Syn accumulations were significantly attenuated in *Gpr37* gKO mice (Figures 2R and 2S).

Taken together, these data suggest that GPR37 deficiency prevents both toxin- and α Syn-aggregate-derived DA neuronal loss, motor impairment, and chronic pain.

PSAP is enriched in DA neurons, and the absence of PSAP alleviates PD-related neurodegeneration

Since GPR37 has been identified as a receptor for PSAP,²² we attempted to investigate the potential contribution of PSAP to the progression of PD. We found that *Psap* was selectively enriched in TH⁺-DA neurons in the SNpc (Figure 3A). Furthermore, PSAP protein levels were obviously elevated in the CSF of 6-OHDA-injected PD mice (Figure 3B).

Figure 2. GPR37 deficiency in oligodendrocytes attenuates 6-OHDA- or hA53T- α Syn-induced neurodegeneration and behavioral deficits
(A and C) Representative TH staining of SNpc DA neurons (scale bar: 200 μ m) and striatum dopaminergic fibers (scale bar: 400 μ m) at 3 weeks after saline or 6-OHDA injection.

- (B) Stereological counts of TH-stained cells in SNpc ($n = 3$ –5).
- (D) Quantification of the relative optical density of TH⁺ striatal dopaminergic fibers. $n = 9$ –12 slices from 3–4 mice per group.
- (E and F) 2 weeks after saline or 6-OHDA injection, APO-induced rotation test and rotarod test were performed. $n = 8$ –17.
- (G and H) 6-OHDA-triggered mechanical allodynia and heat hyperalgesia in WT, *Gpr37* gKO, and CKO mice ($n = 5$ –17).
- (I) Representative TH staining of SNpc DA neurons (scale bar: 100 μ m) at 3 months after AAV-GFP (control) or AAV- α Syn injection.
- (J) Stereological counts of TH⁺ cells (left) and quantification of optical density of TH⁺ striatal dopaminergic fibers (right). $n = 6$ –10.
- (K) Stereological counting of NeuN⁺ neurons in SNpc ($n = 4$ –6).
- (L–O) *Gpr37* deficiency prevented AAV- α Syn-induced behavioral deficits as assessed by rotarod test (L), pole test (M), von Frey test (N), and tail immersion test (O). $n = 6$ –11.
- (P) Representative immunoblots of human α Syn and β -actin in SNpc.
- (Q) Quantification of α Syn level normalized to β -actin. $n = 4$.
- (R) Immunofluorescent staining of p- α Syn and TH in SNpc after 3 months of AAV-GFP and AAV- α Syn injections. Scale bar, 200 μ m.
- (S) Quantification of the relative optical density of p- α Syn in SNpc. $n = 4$ –5.

Bonferroni's one-way ANOVA was used in (B), (D)–(F), (J)–(M), (Q), and (S), and Bonferroni's two-way ANOVA was used in (G), (H), (N), and (O). All data are means \pm SEM. ns, not significant; * $p < 0.05$, ** $p < 0.01$, *** $p < 0.001$, and **** $p < 0.0001$.

To investigate the role of PSAP in the development of PD, we generated *Psap* CKO mice by crossing *Psap*^{f/f} mice (WT) with *TH-Cre* mice³⁵ (Figure 3C). The expression of *Psap* was largely abolished in DA neurons of *Psap* CKO mice compared with WT mice (Figures S3A and S3B). The number of nigral DA neurons and the density of striatal DA fibers in *Psap* CKO mice were comparable to those in WT mice (Figures S3C and S3D). *Psap* CKO mice also exhibited normal motor function and basal pain levels (Figures S3E and S3F). After 6-OHDA injection, *Psap* CKO mice exhibited significantly less loss of DA neurons (Figures 3D and 3E). Compared to WT mice, 6-OHDA-injected *Psap* CKO mice demonstrated significant resistance to behavioral abnormalities (Figures 3F–3I). Similarly, *Psap* CKO mice exhibited a rescue of pathologic α Syn accumulations and DA neuron degeneration (Figures S3G–S3J). AAV- α Syn-injected *Psap* CKO mice also demonstrated significant resistance to motor impairment (Figures S3K and S3L).

To further confirm whether PD-related degeneration is dependent on the local PSAP expression in the SNpc, we conditionally knocked out *Psap* from the SNpc (*Psap* cKO) by stereotactically injecting AAV-Cre-mCherry into the SNpc of *Psap*^{f/f} mice (Figure 3J). *Psap* expression was efficiently ablated in the SNpc of *Psap* cKO mice (Figures S3M–S3O). However, *Psap* cKO mice displayed no deficits in basal motor function (Figures S3P and S3Q) or basal nociception (Figure S3R). Importantly, 6-OHDA-induced DA neuron neurodegeneration were largely abolished in *Psap* cKO mice (Figures 3K and 3L). Furthermore, *Psap*-deficient mice showed notable improvements in accompanying behavioral deficits (Figures S3M–S3P).

Taken together, these results indicate that PSAP is mainly expressed in DA neurons in the substantia nigra and that PD-related DA neurodegeneration is dependent on PSAP.

PSAP evokes upregulation of IL-6 in oligodendrocytes and PD-like dysfunction via GPR37

Previous studies have reported that GPR37 negatively regulates oligodendrocyte differentiation and myelination via osteocalcin application.^{19,20} Interestingly, although *Gpr37* gKO mice showed a higher expression of *Apc* mRNA in the SNpc (Figure S4A), the expression of *Apc*, *Mbp*, and *olig2* mRNA was not significantly different between control and 6-OHDA-injected WT and *Gpr37* gKO mice (Figure S4A). These data suggest that the

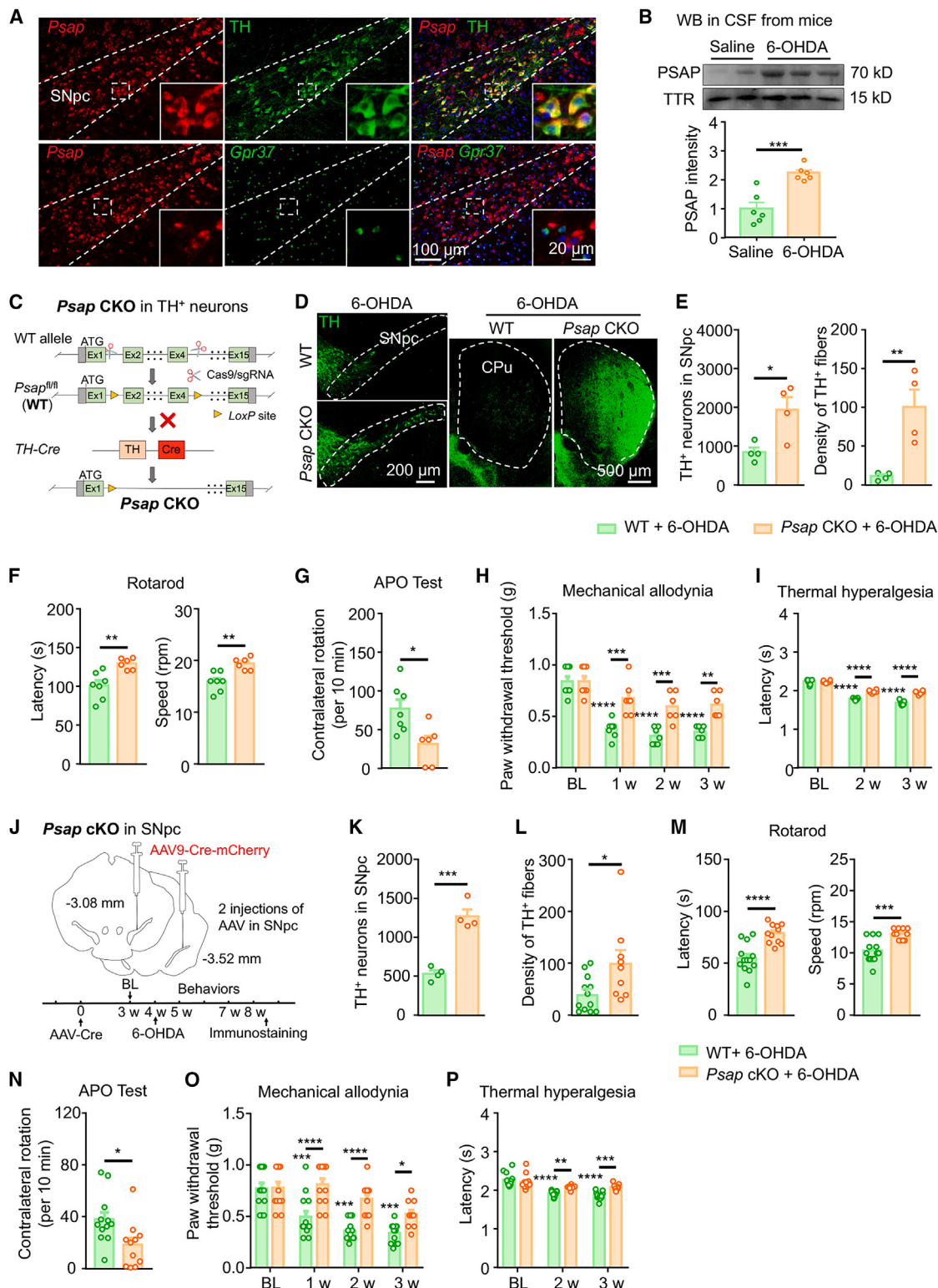


Figure 3. PSAP is enriched in DA neurons, and the absence of PSAP alleviates PD-related neurodegeneration

(A) Colocalization of *Psap* mRNA with TH or *Gpr37* mRNA in SNpc. Scale bars: 100 μm and 20 μm (insets).

(B) Western blot analysis shows PSAP protein is highly elevated in CSF of 6-OHDA-injected mice after 1 week of saline or 6-OHDA injection ($n = 6$).
(C) Schematic illustration of the strategy to conditionally knock out *Psap* (*Psap* CKO) from DA neurons.

(legend continued on next page)

GPR37-mediated modulation of oligodendrocyte differentiation and myelination may not play a major role in PD-like neurodegeneration induced by 6-OHDA.

Recent studies have also shown that oligodendrocytes play a considerable role in neuroinflammation and express various immunomodulatory molecules, including cytokines and chemokines.^{13,36} To investigate the involvement of GPR37 in the immunomodulatory functions of oligodendrocytes, we conducted experiments using primary cultured oligodendrocytes (Figure S4B) as previously described.³⁷ Interestingly, we showed that a PSAP-derived 14-mer peptide (TX-14)³⁸ elicited a robust upregulation of *Il-6* in a dose-dependent manner in primary cultured oligodendrocytes (Figures 4A and S4C). In contrast, treatment with TX-14 failed to induce *Il-6* upregulation in oligodendrocytes derived from *Gpr37* gKO mice (Figure 4B). A previous study showed that GPR37 can evoke ERK (extracellular regulated protein kinases) phosphorylation via the $G\alpha_i$ -dependent signaling pathway upon TX-14 stimulation,²² which was blocked by the $G\alpha_i$ inhibitor PTX (Pertussis toxin) (Figures S4D and S4E). As shown in Figure S4F, both PTX and MEK (mitogen-activated protein kinase kinase) inhibitor U0126 exhibited inhibitory effects on the upregulation of *Il-6* induced by TX-14 (Figure S4F). These results indicate that the PSAP analog induces the upregulation of *Il-6* in oligodendrocytes via the GPR37/ $G\alpha_i$ /MEK pathway.

Next, we investigated whether treatment with the PSAP analog TX-14 could be sufficient to induce neurodegeneration and PD-like dysfunction. Notably, WT mice unilaterally treated with TX-14 exhibited a significant decrease in SNpc DA neurons compared to the control and *Gpr37* KO mice (Figures 4C–4E). TX-14 treatment also resulted in a significant impairment of movement coordination (Figure 4F) and mechanical allodynia in WT mice but not *Gpr37* KO mice (Figure S4G). Thus, the PSAP analog induces neurodegeneration and PD-like dysfunctions in a GPR37-dependent manner.

IL-6 from oligodendrocytes is critical for the development of PD-like neurodegeneration

Several studies in both humans and mice showed that IL-6 was elevated in peripheral blood and the brain in PD.^{39–41} Similar to previous reports, we observed an increase in *Il-6* mRNA expression in the SNpc of WT mice 1 week after 6-OHDA injection (Figure 4G). However, this increase in *Il-6* expression was abolished in 6-OHDA-injected *Gpr37* gKO mice (Figure 4G). Consistently, IL-6 protein levels showed an elevation in the SNpc (Figure 4H) and CSF (Figure 4I) of WT PD mice following 6-OHDA administration but not in those of 6-OHDA-treated GPR37-deficient mice (Figures 4H and 4I).

To determine the specific role of IL-6 derived from oligodendrocytes in 6-OHDA-induced neurodegeneration, we utilized AAV expressing *Il-6* short hairpin RNA (shRNA) in a Cre-dependent manner (AAV-DIO-sh*Il-6*-mCherry) in *Pip1-Cre/ER* mice (Figure 4J). The expression of mCherry-sh*Il-6* was predominantly observed in olig2⁺ oligodendrocytes (Figure S4H). The knockdown of *Il-6* in oligodendrocytes had no significant effect on basal motor function or nociception (Figures S4I–S4K). After the unilateral injection of 6-OHDA, *Il-6* knockdown mice showed a substantial rescue of DA neuron loss (Figure 4K). The knockdown of IL-6 in oligodendrocytes also significantly prevented the motor deficits (Figures 4L and 4M) and mechanical allodynia (Figure S4L) induced by 6-OHDA. These data suggest that IL-6 from oligodendrocytes is essential for DA neuronal loss, motor impairment, and chronic pain in PD mice.

Next, we investigated whether and how IL-6 is capable of inducing PD-like symptoms. We treated WT mice unilaterally with injections of recombinant IL-6 protein in the SNpc and compared them to control mice treated with saline (Figure 4N). Our results showed that mice treated with IL-6 exhibited a significant decrease in SNpc DA neurons, as well as a decrease in the optical density of TH⁺ fibers in the CPu (Figures 4O and 4P). Additionally, IL-6 treatment resulted in a significant impairment in movement coordination (Figure 4Q) and mechanical allodynia (Figure 4M). Since microglial and astrocytic activation are pathological hallmarks of neuroinflammation in the substantia nigra in PD,¹² microgliosis and astrogliosis were evaluated through immunohistochemistry and qPCR. Both Iba1 and GFAP were markedly increased in IL-6-injected mice, indicating an enhanced neuroinflammatory response in the SNpc (Figures 4R and 4S). Furthermore, we observed microglial and astrocyte activation in the ipsilateral SNpc of WT mice injected with 6-OHDA (Figures S5A–S5D). However, the glial activation was largely blunted in *Gpr37* gKO and CKO mice, which lack GPR37 within oligodendrocytes (Figures S5A–S5D) and fail to upregulate IL-6 in the SNpc (Figures 4G–4I). Moreover, both microgliosis and astrogliosis induced by 6-OHDA were relieved in *Psap* CKO mice (Figures S5E and S5F) or by the knockdown of *Il-6* in oligodendrocytes (Figures S5G and S5H), suggesting the important role of the PSAP-GPR37-IL-6 axis for the neuroinflammation in PD mice. Together, these data suggest that IL-6 in the SNpc is sufficient to induce neuroinflammation, DA neuronal loss, motor impairment, and chronic pain.

A recent study found that IL-6 could induce a toxic neuronal response via the *trans*-signaling pathway, in which the soluble form of the IL-6 receptor (IL-6R) binds to secreted IL-6 to form a complex that interacts with glycoprotein 130 (gp130; encoded

(D) TH staining of SNpc DA neurons (left, scale bar: 200 μ m) and striatum dopaminergic fibers (right, scale bar: 500 μ m) at 3 weeks after 6-OHDA injection.
(E) Stereological counts of TH⁺ cells (left) and quantification of optical density of TH⁺ striatal dopaminergic fibers (right). $n = 4$.

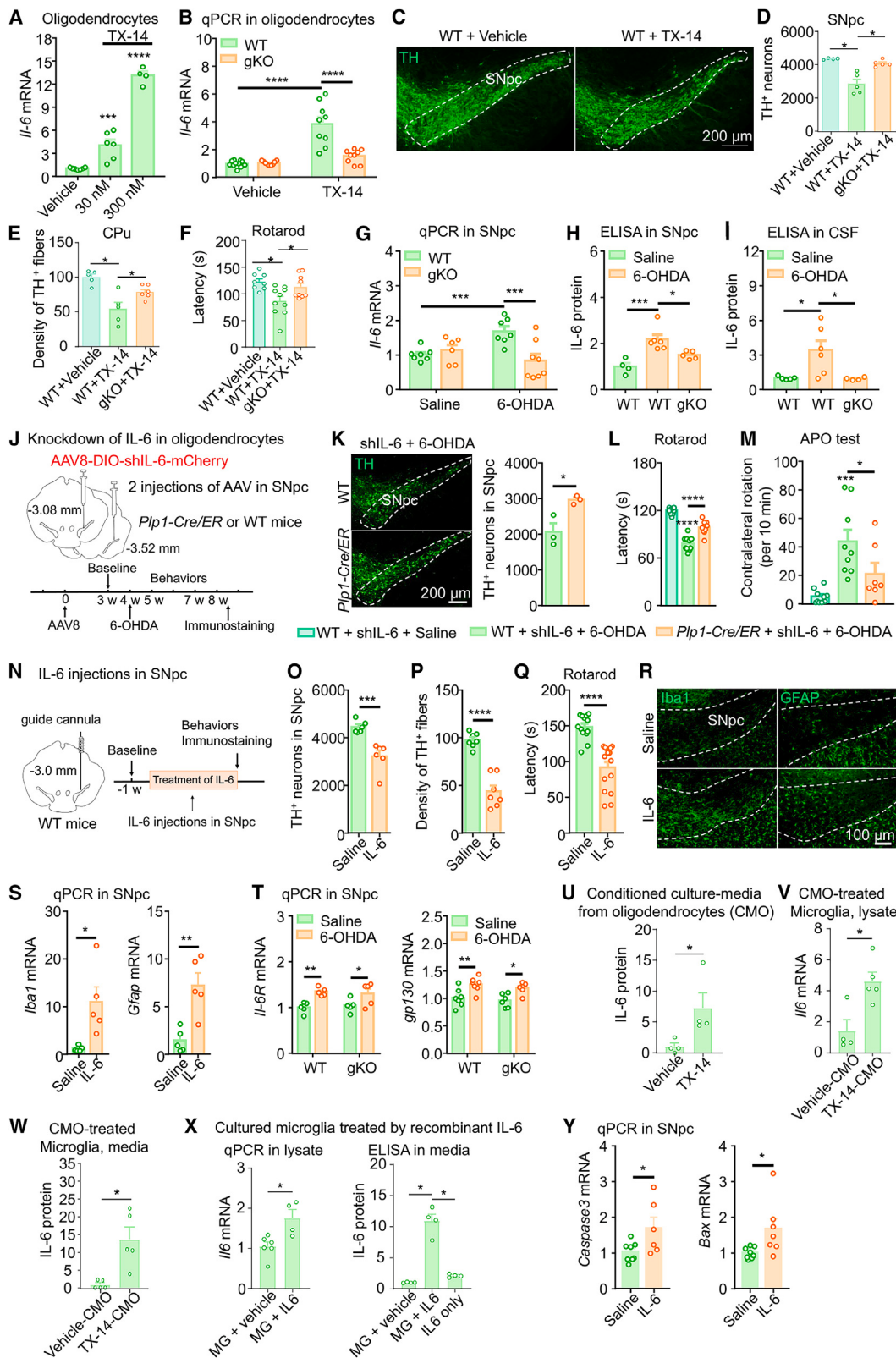
(F–I) *Psap* CKO mice exhibit diminished 6-OHDA-induced behavioral deficits as assessed by rotarod test (F), APO-induced rotation test (G), von Frey test (H), and tail immersion test (I). $n = 6$ –7.

(J) Schematic illustration of the strategy to conditionally knock out *Psap* from SNpc (*Psap* cKO) by stereotaxic injecting AAV-Cre-mCherry into *Psap*^{f/f} mice SNpc.

(K and L) *Psap* cKO mice exhibit largely abolished DA neurons loss (K, $n = 4$) and TH⁺ optical density decrease (L; $n = 9$ –12 slices from 3–4 mice) induced by 6-OHDA injection.

(M–P) *Psap* cKO mice exhibit significantly attenuated 6-OHDA-induced behavioral deficits as assessed by rotarod test (M), APO-induced rotation test (N), von Frey test (O) and tail immersion test (P). $n = 11$ –13.

Two-tailed Student's unpaired *t* test was used in (B), (E)–(G), and (K)–(N), and two-way ANOVA followed by Bonferroni's post hoc test was used in (H), (I), (O), and (P). All data are means \pm SEM. * $p < 0.05$, ** $p < 0.01$, *** $p < 0.001$, and **** $p < 0.0001$.



(legend on next page)

by *Il-6st*) to mediate intracellular signal transduction.⁴² To test whether IL-6 could directly induce damage to DA neurons, we first examined whether DA neurons express *Il-6R* and *gp130* using *in situ* hybridization. As shown in Figure S5I, *gp130* mRNA, but not *Il-6R* mRNA, colocalized well with TH. Both *gp130* and *Il-6R* mRNA were expressed in *Iba1*⁺ microglia (Figure S5I). The expression of *Il-6R* and *gp130* mRNA was also significantly increased in the SNpc of WT and *Gpr37* gKO mice with 6-OHDA-induced PD (Figure 4T). To explore the potential contribution of microglia to the IL-6 elevation triggered by the initial oligodendrocyte-derived IL-6, we further investigated whether conditioned culture media from oligodendrocytes (CMOs) could induce more IL-6 release in cultured microglia. Treatment with the PSAP analog TX-14 elicited IL-6 release in CMOs (Figure 4U). Importantly, TX-14-treated CMOs could induce robust IL-6 upregulation (Figure 4V) and release (Figure 4W) in cultured microglia. Similarly, direct treatment with recombinant IL-6 protein also significantly induced IL-6 upregulation and release (Figure 4X) in cultured microglia. Interestingly, IL-6 injection in the SNpc could also promote the expression of *Caspase 3* and *Bax* (Figure 4Y), which have been suggested to mediate apoptotic degradation.⁴³ These data suggest that the initial IL-6 from oligodendrocytes triggers microglial activation and produces more IL-6, which could contribute to the enhanced neuroinflammation and DA neuronal degeneration.

Collectively, our results demonstrate that IL-6 from oligodendrocytes is critical for 6-OHDA-induced neuroinflammation, DA neuronal loss, motor impairment, and chronic pain in PD mice.

GPR37 deletion in oligodendrocytes at an early stage rescues neurodegeneration in parkinsonian mice

We next asked whether inhibiting oligodendrocytic GPR37 at an early stage could provide protection against the loss of

DA neurons in parkinsonian mice. GPR37 in oligodendrocytes was selectively knocked out by intraperitoneally injecting tamoxifen (TAM) into *p/p1-Cre/ER;Gpr37*^{f/f} (CKO) mice 3 weeks after unilateral AAV- α Syn injection, a stage with widespread expression of hA53T- α Syn in the substantia nigra (Figure 5A).^{44,45} *Gpr37* CKO mice treated with TAM showed a significantly lower decrease in nigral DA neurons and ipsilateral striatal TH⁺ optical density after a unilateral injection of AAV- α Syn compared with TAM-treated *Gpr37*^{f/f} (WT) mice (Figures 5B–5D). Furthermore, TAM-treated CKO mice exhibited a significant prevention of motor impairment, mechanical allodynia, and thermal hyperalgesia induced by AAV- α Syn injection (Figures 5E–5G). Although the expression of total α Syn remained equivalent across all conditions (Figures 5H and 5I), pathologic α Syn accumulations were significantly rescued in *Gpr37* CKO mice (Figure 5J).

Taken together, these results demonstrate that GPR37 deletion in oligodendrocytes at an early stage protects against neurodegeneration in hA53T- α Syn-induced PD model mice.

Hallmarks of the PSAP-GPR37-IL-6 axis are observed in patients with PD

Finally, we asked whether our findings have translational potential for the clinical treatment of PD. To explore the possible relevance of GPR37 in human PD, an snRNA-seq dataset²¹ of postmortem SNpc from patients with PD was utilized. Seven distinct cell populations within the SNpc, including oligodendrocytes and DA neurons, were identified by clustering analysis with the indicated cell-type-specific genes (Figures S6A and S6B). We found that *GPR37* was specifically expressed in oligodendrocytes in the SNpc from patients with PD and controls (Figures 6A and 6B). *In situ* hybridization using

Figure 4. PSAP evokes IL-6 upregulation in oligodendrocytes, and oligodendrocyte-derived IL-6 is required for the development of PD-like neurodegeneration

- (A) PSAP analog TX-14 leads to greater increase of *Il-6* mRNA in a dose-dependent manner in primary cultured oligodendrocytes. *n* = 4–7.
 - (B) qPCR analysis of *Il-6* mRNA in primary cultured oligodendrocytes. *n* = 9–11.
 - (C) Immunofluorescent staining of DA neurons in SNpc from vehicle- or TX-14-injected mice. Scale bar: 200 μ m.
 - (D) Stereological counts of TH⁺ neurons in SNpc. *n* = 4–5.
 - (E) Quantification of the relative optical density of TH⁺ striatal dopaminergic fibers. *n* = 5–6.
 - (F) Motor function was tested by rotarod test. *n* = 8–10.
 - (G) qPCR analysis of *Il-6* mRNA in SNpc tissues. *n* = 6–7.
 - (H and I) ELISA analysis of IL-6 protein level in SNpc (H) and CSF (I) after 1 week of saline or 6-OHDA injection. *n* = 4–6.
 - (J) Schematic for stereotaxic injection paradigm and timeline of behavioral tests and tissues collection.
 - (K) Immunofluorescent staining (scale bar: 200 μ m) and stereological counts of TH⁺ cells in SNpc after 3 weeks of 6-OHDA injection. *n* = 3.
 - (L and M) IL-6 knockdown mice exhibit significant prevention for 6-OHDA-induced motor deficits as assessed by rotarod test (L) and APO-induced rotation test (M). *n* = 7–10.
 - (N) Schematic for stereotaxic injection and timeline paradigm.
 - (O and P) Quantification of TH⁺ DA neurons in SNpc (O) and optical density of DA fibers in striatum (P). *n* = 6–7.
 - (Q) 12 days after nigral saline or recombinant IL-6 protein injection, rotarod test was performed. *n* = 13–15.
 - (R and S) Immunofluorescent staining with *Iba1* and GFAP (R, scale bar: 100 μ m) and qPCR analysis (S, *n* = 5) of *Iba1* and *Gfap* mRNA in SNpc.
 - (T) qPCR analysis of *gp130* and *Il-6R* mRNA in SNpc after 1 week of saline or 6-OHDA injection. *n* = 5–7.
 - (U) ELISA analysis of IL-6 protein level in conditioned culture media from oligodendrocytes (CMOs) after TX-14 treatment (TX-14-CMOs). *n* = 4.
 - (V) *Il-6* mRNA was significantly increased in TX-14-CMO-cultured microglia compared with vehicle-CMO-cultured microglia, as measured by qPCR analysis. *n* = 4–5.
 - (W) IL-6 protein was significantly elevated in TX-14-CMOs after being cultured with microglia. *n* = 5.
 - (X) Recombinant IL-6 treatment led to increase of *Il-6* mRNA (left) and IL-6 protein (right) in primary cultured microglia compared with vehicle treatment. *n* = 4–6.
 - (Y) qPCR analysis of *Caspase3* and *Bax* mRNA in SNpc. *n* = 7–8.
- One-way ANOVA followed by Bonferroni's post hoc test was used in (A), (D)–(F), (H), (I), (L), (M), and (X) (right), Bonferroni's two-way ANOVA was used in (B), (G), and (T), and two-tailed Student's unpaired t test was used in (K), (O)–(Q), (S), (U)–(X) (left), and (Y). All data are means \pm SEM. **p* < 0.05, ***p* < 0.01, ****p* < 0.001, and *****p* < 0.0001.

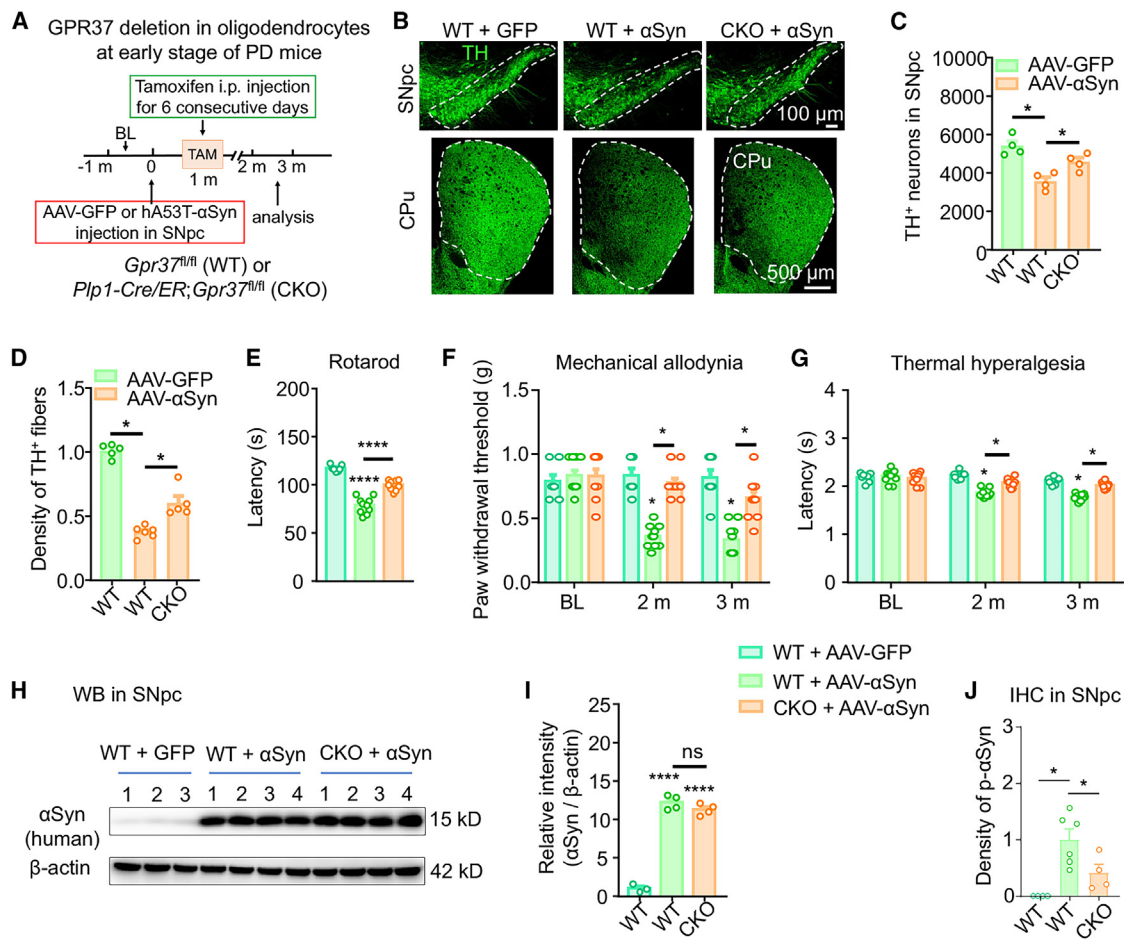


Figure 5. GPR37 deletion in oligodendrocytes at an early stage rescues neurodegeneration in parkinsonian mice

(A) Schematic for timeline paradigm.
 (B) Representative TH staining of SNpc DA neurons (scale bar: 100 μ m) and striatum dopaminergic fibers (scale bar: 500 μ m).
 (C) Stereological counts of TH-stained cells in SNpc. $n = 4$.
 (D) Quantification of the relative optical density of TH⁺ striatal dopaminergic fibers. $n = 5-6$.
 (E) 3 months after AAV-GFP or α Syn injection in WT and CKO mice treated with TAM, rotarod test was performed.
 (F and G) Mechanical allodynia and thermal hyperalgesia were detected at the indicated time. $n = 7-10$ in E-G.
 (H) Representative immunoblots of human α Syn and β -actin in SNpc.
 (I) Quantification of α Syn level normalized to β -actin. $n = 3-4$.
 (J) Quantification of the relative optical density of p- α Syn in SNpc. $n = 4-6$.
 $n = 7-10$ in (E)-(G). One-way ANOVA followed by Bonferroni's post hoc test was used in (C)-(E), (I), and (J), and two-way ANOVA followed by Bonferroni's post hoc test was used in (F) and (G). All data are means \pm SEM. ns, not significant, * $p < 0.05$, and *** $p < 0.0001$. i.p., intraperitoneal; TAM, tamoxifen.

fresh-frozen midbrain sections confirmed that *GPR37* mRNA was primarily observed in *PLP1*⁺ oligodendrocytes but not DA neurons (Figures 6C, S6C, and S6D). Consistent with our findings in mice, *GPR37* within the oligodendrocytes showed a remarkable elevation in the SNpc from patients with PD (Figures 6B, 6D, and 6E). Moreover, *GPR37* expression levels were significantly increased in another independent cohort^{46,47} of patients with PD (Figure S6E). These findings indicate the potential relevance of oligodendrocytic GPR37 in human PD.

Furthermore, PSAP mRNA was enriched in DA neurons in human brain sections, (Figure 6F), and PSAP protein was significantly increased in CSF from patients with PD (Figure 6G). We

then compared IL-6 levels in CSF samples using ELISA and found that IL-6 protein was obviously elevated in CSF from patients with PD (Figure 6H) compared with controls. We also found that the expression of *gp130* mRNA was significantly increased in the SNpc of patients suffering from sporadic PD (Figure 6I). In addition, abnormal activation of microglia and astrocytes was detected in SNpc sections from patients with PD (Figures 6J and 6K).

Thus, we confirmed the expression of PSAP and GPR37 in human postmortem SNpc and the elevated levels of PSAP and IL-6 in CSF from patients with PD, suggesting the potential relevance of the PSAP-GPR37-IL-6 signaling axis in the clinical manifestation of PD.

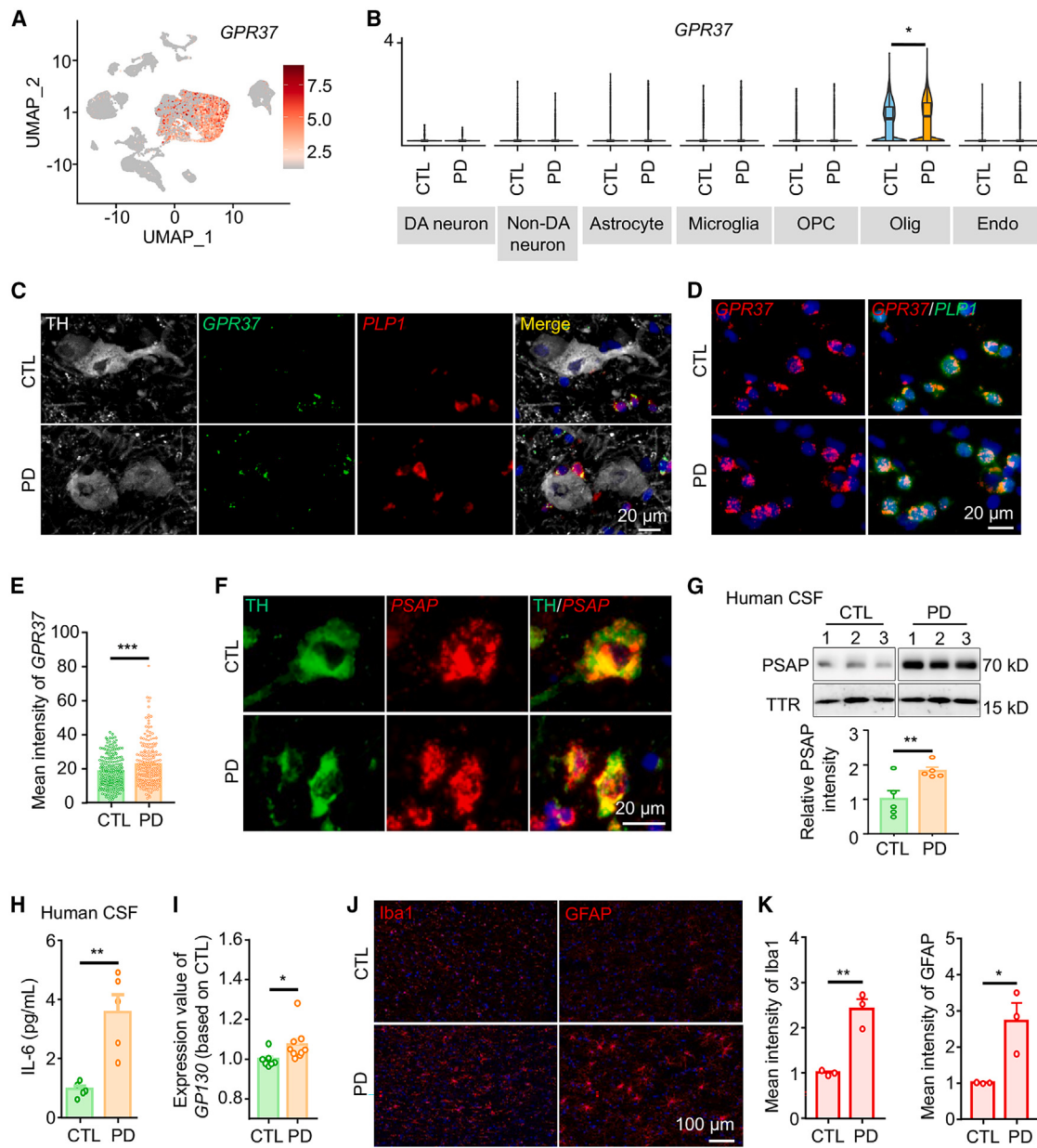


Figure 6. Hallmarks of the PSAP-GPR37-IL-6 axis are observed in patients with PD

- (A) Uniform manifold approximation and projection (UMAP) plot of *GPR37* expression re-analyzed from a published snRNA-seq dataset by Kamath et al.²¹
- (B) Violin plot of *GPR37* expression exhibits significantly increased *GPR37* within the oligodendrocyte of SNpc from patients with PD compared with controls (CTLs).
- (C) Colocalization of human *GPR37* mRNA with TH and *PLP1* mRNA in postmortem SNpc. Scale bar: 20 μm.
- (D) *In situ* hybridization of human *GPR37* mRNA with *PLP1* mRNA in SNpc. Scale bar: 20 μm.
- (E) Quantification of the relative optical density of *GPR37* mRNA within *PLP1*⁺ oligodendrocytes. $n = 199\text{--}220$ cells.
- (F) Colocalization of human *PSAP* mRNA with TH in postmortem SNpc. Scale bar: 20 μm.
- (G) Representative immunoblots of PSAP and TTR in human CSF. Bottom, quantification of PSAP level normalized to TTR. $n = 6\text{--}8$.
- (H) ELISA analysis of IL-6 protein level in CSF from patients with PD and age-matched CTLs. $n = 5$.
- (I) *GP130* mRNA levels in lateral substantia nigra of healthy CTLs and patients with sporadic PD from GEO: GSE8397. $n = 7\text{--}9$.
- (J) Representative Iba1 and GFAP staining in postmortem SNpc. Scale bar: 100 μm.
- (K) Quantification of the relative optical density of Iba1 and GFAP in SNpc. $n = 3$.
- Two-tailed Student's unpaired t test was used. All data are means \pm SEM. * $p < 0.05$, ** $p < 0.01$, and *** $p < 0.001$. CTL, control; DA, dopaminergic; non-DA, non-dopaminergic; OPC, oligodendrocyte precursor cell; Olig, oligodendrocyte; Endo, endothelial cells.

DISCUSSION

In this study, we discovered that oligodendrocytes drive neuroinflammation and DA neuronal loss in PD through GPR37-mediated IL-6 production. CKO of GPR37 in oligodendrocytes prevents DA neurodegeneration and behavioral impairment in multiple models of PD. In addition, PSAP, as an endogenous ligand of GPR37, is enriched in DA neurons, and its secretion is increased in CSF, which further triggers the production of IL-6 from oligodendrocytes via GPR37 signaling, leading to DA neurodegeneration in PD. Importantly, targeted ablation of GPR37 in oligodendrocytes at an early stage rescued neurodegeneration in parkinsonian mice.

GPR37 is enriched in the brains of both humans and rodents.^{19,48} The highest GPR37 mRNA levels are expressed in the substantia nigra and CC within the human brain.^{49,50} Immunohistochemical staining of GPR37 in the mouse brain suggested that neuronal GPR37 protein was primarily restricted to nigral DA neurons and hippocampal neurons, whereas glial expression was highly enriched in oligodendrocytes.¹⁸ However, immunohistochemical results are really dependent on the specificity of the GPR37 antibody. Here, we describe a different expression pattern of GPR37 in which the receptor is selectively expressed in oligodendrocytes, but not DA neurons, through snRNA-seq analysis and *in situ* hybridization. We also confirmed this unique distribution pattern by using the transgenic mouse line, which contains a bacterial LacZ reporter gene in the *Gpr37* locus.^{19,20,23,38}

GPR37 has been identified as a substrate for parkin and aggregates abnormally in patients with autosomal recessive juvenile parkinsonism, triggering the unfolded protein response and death of DA neuronal cells.^{17,18,51} However, the precise function of GPR37 in PD pathogenesis and progression remains elusive. GPR37 expression is increased in the nigrostriatal system of experimental parkinsonism and patients with sporadic PD,^{52,53} and ecto-GPR37 peptides are augmented in the CSF from patients with PD but not increased in patients with Alzheimer's disease.⁵² We revealed that GPR37 abolishment within oligodendrocytes prevents 6-OHDA-intoxication- and α Syn-aggregate-induced DA neuronal loss and behavioral deficiency, consistent with a previous study showing that GPR37 gKO mice exhibit a resistant phenotype to MPTP (1-methyl-4-phenyl-1,2,3,6-te-trahydropyridine) toxin.⁵⁴ These results indicate that GPR37 within oligodendrocytes, but not DA neurons, contributes to neurodegeneration in PD.

GPR37 has been postulated to be a receptor for PSAP, which is a multifunctional protein that plays roles both extracellularly as a secreted factor and intracellularly as a regulator of lysosomal enzyme function.^{22,55,56} Although multiple genetic studies have indicated that PSAP might be involved in the PD,⁵⁷ its precise mechanism is complex and remains elusive. We found that PSAP is enriched in DA neurons of the SNpc, while the protein synthesis of PSAP was not upregulated in PD patient-derived cells.⁵⁸ In the lysosome, PSAP is generated into four lysosomal activator proteins known as saposins A–D, which assist in glucosylceramide degradation.^{59,60} The knockdown of PSAP in human induced pluripotent stem cell (iPSC)-derived neurons leads to neuronal ferroptosis in response to oxidative stress.⁶¹ Recent

reports suggest that variants in the saposin D domain of PSAP, which is required for lysosomal transport of the PSAP protein, are risk factors for PD.^{62,63} Intriguingly, we found that secreted PSAP could be implicated in PD neurodegenerative pathogenesis, consistent with a recent study⁶⁴ that showed that an increased PSAP level in CSF is positively correlated with PD-related motor impairments, the cardinal feature in patients with PD. Notably, the PSAP analog TX-14 induced neurodegeneration and PD-like dysfunctions in a GPR37-dependent manner (Figures 4C–4F). Taking these results together, it seems that the increased PSAP level in CSF (extracellular PSAP) is detrimental and causes PD-related dysfunctions via the activation of GPR37 signaling and subsequent neuroinflammation.

Although growing evidence suggests the possible implication of oligodendrocytes in PD,⁶⁵ oligodendrocytes have received much less attention in PD than in multiple system atrophy.²⁵ A recent study integrating genome-wide association study results with single-cell transcriptomic data from the mouse nervous system indicated an unexpected role of oligodendrocytes in PD.¹⁵ Moreover, genes upregulated in PD are significantly enriched in oligodendrocytes, and alterations in oligodendrocytes occur at an early stage of disease progression, which precedes neurodegeneration in the SNpc.¹⁵ Interestingly, we found that the expression of *Gpr37* and *Il-6* mRNA was highly increased in oligodendrocytes in WT PD mice before motor dysfunctions were exhibited. Consistently, the CKO of GPR37 in oligodendrocytes at an early stage rescued neurodegeneration in parkinsonian mice. In addition, EM data showed that deleting GPR37 in oligodendrocytes did not change the integrity of myelin and associated axons, suggesting the myelin-independent role of oligodendrocytes in triggering neuroinflammation and neurodegeneration in PD.

IL-6 utilizes classic or *trans*-signaling pathways to mediate its biological effects.⁶⁶ The classic signaling pathway is mediated via the membrane-bound IL-6R. However, cells that do not express IL-6R can initiate IL-6 signaling via the *trans*-signaling pathway.^{67,68} Although IL-6R expression is restricted to a few cells, gp130 is ubiquitously expressed in multiple cell types, including neurons.^{69,70} As expected, we found that *gp130*, but not *Il-6R*, was expressed in DA neurons and significantly increased in the SNpc after 6-OHDA injection. We also revealed that recombinant IL-6 protein injection could induce the apoptosis of DA neurons, consistent with a recent study showing that IL-6 could induce a cellular iron sequestration response via its *trans*-signaling pathway, contributing to synuclein-induced neurodegeneration.⁴² Furthermore, the conditional knockdown of IL-6 within oligodendrocytes rescued neurodegeneration in PD mice. These data indicate that IL-6 from oligodendrocytes is a key player in PD pathogenesis. Since both *Il-6R* and *gp130* mRNA were expressed in microglia and significantly increased in the SNpc of PD mice, it seems that oligodendrocyte-derived IL-6 could be an important trigger for microglial activation, which further contributes to neuroinflammation and mediates oligodendrocyte-induced neuronal loss in PD. Thus, we propose that the initial IL-6 from oligodendrocytes could trigger microglial activation via IL-6R signaling and produce more IL-6; this positive feedback would contribute to the enhanced neuroinflammation, DA neuronal degeneration, and PD-related dysfunctions.

In summary, we present evidence for a new mechanistic insight into the role of oligodendrocytes, as the immunomodulatory glia, in the pathogenesis of PD. We demonstrate that GPR37 is specifically expressed in oligodendrocytes and significantly upregulated in both patients with PD and PD mouse models. Furthermore, we found that PSAP secretion is increased in the CSF from patients with PD. This promotes the production of IL-6 from oligodendrocytes via GPR37 signaling, which further causes neuroinflammation and DA neuron loss. Our findings indicate that oligodendrocytes drive neuroinflammation and neurodegeneration in PD via the PSAP-GPR37-IL-6 axis (Figure S7). Moreover, we confirmed the enriched expression of PSAP in human DA neurons and the increased secretion of PSAP and IL-6 in CSF from patients with PD. Thus, therapeutic strategies targeting the PSAP-GPR37-IL-6 axis might relieve disease progression in patients with PD.

Limitations of the study

PSAP is a glycosylated protein with dual functions: an intracellular form that regulates lysosomal enzyme function and an extracellular form that acts as a secreted factor. Although we found that increased PSAP secretion in CSF is detrimental and could cause PD-related dysfunction via the activation of GPR37 signaling, we did not dissect the specific contribution of intracellular PSAP in the degeneration of DA neurons in PD models. A recent study⁶⁴ found a slow but progressive DA reduction and TH loss in cPSAP^{DAT} CKO (CKO of PSAP in DA neurons) mice at a late stage (8–16 months), which was significant at the 16-month mark. However, for *Psap* CKO mice that were 4 months old or younger, their data⁶⁴ are consistent with our study that the CKO of PSAP in DA neurons does not impair the DA signals or motor functions. It seems that intracellular PSAP could have a protective role, especially at a late stage, and that it might be involved in a GPR37-independent pathway. Thus, further study is warranted to investigate the role of lysosomal PSAP in the pathogenesis of PD. Another limitation is that while we observed that initial IL-6 from oligodendrocytes could trigger microglial activation and produce more IL-6, we did not identify how much the microglia contribute to the IL-6 level. Future studies are needed to investigate the expression pattern of IL-6 in PD models and whether IL-6 in microglia is a key factor for PD pathogenesis.

RESOURCE AVAILABILITY

Lead contact

Further information and requests for resources should be directed to and will be fulfilled by the lead contact, Dr. Zhen-Zhong Xu (xuzz@zju.edu.cn).

Materials availability

This study did not generate new unique reagents.

Data and code availability

All data associated with this study are present in the paper or the [supplemental information](#). The accession numbers for the sequencing data re-analyzed in this study are listed in the [key resources table](#).

This paper does not report original code.

Any additional information required to analyze the data reported in this paper is available from the [lead contact](#) upon reasonable request.

ACKNOWLEDGMENTS

The authors thank Dr. Kedjiang Ye (CAS) and Dr. Ru-Rong Ji (Duke University) for discussing the manuscript. We are grateful to Drs. Aimin Bao, Yi Shen, and Peiran Jiang at the National Human Brain Bank for Health and Disease, Dr. Sanhua Fang at the Core Facilities of Zhejiang University School of Medicine, and Yuchen Zhang at the Center of Cryo-Electron Microscopy (CCEM) of Zhejiang University for technical assistance. This study was supported by the National Key R&D Program of China (2021ZD0202703 to Z.-Z.X.), the National Natural Science Foundation of China (82101322 to Q.M.; 81971050, 82171206, and 31771162 to Z.-Z.X.; 82301397 to J.Y.; and 81901122 to R.G.), the Zhejiang Provincial Natural Science Foundation of China (LZ18C090002 to Z.-Z.X., LGD22H070004 to R.G., and LGF20H310004 to S.L.), and the MOE Frontier Science Center for Brain Science & Brain-Machine Integration, Zhejiang University. This study was also supported by the Fundamental Research Funds for the Central Universities (2023ZFJH01-01, 2024ZFJH01-01, and 226-2022-00227).

AUTHOR CONTRIBUTIONS

Q.M., J.-L.T., and Y.L. performed the majority of the experiments, analyzed the data, and prepared the figures. R.G. contributed to the interview and CSF collection in patients with Parkinson's disease. X.-R.M. assisted in the primary culture of mouse OPCs. J.-B.W. assisted in the EM experiment. J.Y. performed some of the *in situ* hybridization. B.-J.T. assisted in the cell culture experiment. S.L., M.Q., S.D., J.-W.Z., and J.Z. provided resources and intellectual input for the study. Q.M. and Z.-Z.X. designed the study and prepared the manuscript with input from all authors. Z.-Z.X. supervised the project.

DECLARATION OF INTERESTS

The authors declare no competing interests.

STAR METHODS

Detailed methods are provided in the online version of this paper and include the following:

- [KEY RESOURCES TABLE](#)
- [EXPERIMENTAL MODEL AND STUDY PARTICIPANT DETAILS](#)
 - Animals
 - Cell cultures
 - Human postmortem substantia nigra sections and CSF samples
- [METHOD DETAILS](#)
 - Viral vectors
 - Stereotaxic surgery
 - Immunofluorescence
 - *In situ* hybridization
 - Plasmid construction and transfection
 - Quantitative real-time PCR
 - Assessment of protein secretion
 - Western Blot
 - ELISA
 - Behavioral scheme
 - Transmission electron microscopy
 - Clustering cell into subtypes
- [QUANTIFICATION AND STATISTICAL ANALYSIS](#)
 - Statistical analyses

SUPPLEMENTAL INFORMATION

Supplemental information can be found online at <https://doi.org/10.1016/j.celrep.2025.115266>.

Received: November 15, 2023

Revised: October 28, 2024

Accepted: January 15, 2025

Published: February 4, 2025

REFERENCES

1. Armstrong, M.J., and Okun, M.S. (2020). Diagnosis and Treatment of Parkinson Disease: A Review. *JAMA* 323, 548–560. <https://doi.org/10.1001/jama.2019.22360>.
2. Bloem, B.R., Okun, M.S., and Klein, C. (2021). Parkinson's disease. *Lancet* 397, 2284–2303. [https://doi.org/10.1016/S0140-6736\(21\)00218-X](https://doi.org/10.1016/S0140-6736(21)00218-X).
3. Ye, H., Robak, L.A., Yu, M., Cykowski, M., and Shulman, J.M. (2023). Genetics and Pathogenesis of Parkinson's Syndrome. *Annu. Rev. Pathol.* 18, 95–121. <https://doi.org/10.1146/annurev-pathmechdis-031521-034145>.
4. Chaudhuri, K.R., and Schapira, A.H.V. (2009). Non-motor symptoms of Parkinson's disease: dopaminergic pathophysiology and treatment. *Lancet Neurol.* 8, 464–474. [https://doi.org/10.1016/S1474-4422\(09\)70068-7](https://doi.org/10.1016/S1474-4422(09)70068-7).
5. Schapira, A.H.V., Chaudhuri, K.R., and Jenner, P. (2017). Non-motor features of Parkinson disease. *Nat. Rev. Neurosci.* 18, 435–450. <https://doi.org/10.1038/nrn.2017.62>.
6. Xiang, J., Tao, Y., Xia, Y., Luo, S., Zhao, Q., Li, B., Zhang, X., Sun, Y., Xia, W., Zhang, M., et al. (2023). Development of an alpha-synuclein positron emission tomography tracer for imaging synucleinopathies. *Cell* 186, 3350–3367.e19. <https://doi.org/10.1016/j.cell.2023.06.004>.
7. Panicker, N., Ge, P., Dawson, V.L., and Dawson, T.M. (2021). The cell biology of Parkinson's disease. *J. Cell Biol.* 220, e202012095. <https://doi.org/10.1083/jcb.202012095>.
8. Zhang, Y., Roy, D.S., Zhu, Y., Chen, Y., Aida, T., Hou, Y., Shen, C., Lea, N.E., Schroeder, M.E., Skaggs, K.M., et al. (2022). Targeting thalamic circuits rescues motor and mood deficits in PD mice. *Nature* 607, 321–329. <https://doi.org/10.1038/s41586-022-04806-x>.
9. Chen, Y., Hong, Z., Wang, J., Liu, K., Liu, J., Lin, J., Feng, S., Zhang, T., Shan, L., Liu, T., et al. (2023). Circuit-specific gene therapy reverses core symptoms in a primate Parkinson's disease model. *Cell* 186, 5394–5410.e18. <https://doi.org/10.1016/j.cell.2023.10.004>.
10. Hirsch, E.C., Jenner, P., and Przedborski, S. (2013). Pathogenesis of Parkinson's disease. *Mov. Disord.* 28, 24–30. <https://doi.org/10.1002/mds.25032>.
11. Kam, T.I., Hinkle, J.T., Dawson, T.M., and Dawson, V.L. (2020). Microglia and astrocyte dysfunction in parkinson's disease. *Neurobiol. Dis.* 144, 105028. <https://doi.org/10.1016/j.nbd.2020.105028>.
12. Hirsch, E.C., and Hunot, S. (2009). Neuroinflammation in Parkinson's disease: a target for neuroprotection? *Lancet Neurol.* 8, 382–397. [https://doi.org/10.1016/S1474-4422\(09\)70062-6](https://doi.org/10.1016/S1474-4422(09)70062-6).
13. Zhou, B., Zhu, Z., Ransom, B.R., and Tong, X. (2021). Oligodendrocyte lineage cells and depression. *Mol. Psychiatry* 26, 103–117. <https://doi.org/10.1038/s41380-020-00930-0>.
14. Kirby, L., Jin, J., Cardona, J.G., Smith, M.D., Martin, K.A., Wang, J., Strasburger, H., Herbst, L., Alexis, M., Karnell, J., et al. (2019). Oligodendrocyte precursor cells present antigen and are cytotoxic targets in inflammatory demyelination. *Nat. Commun.* 10, 3887. <https://doi.org/10.1038/s41467-019-11638-3>.
15. Bryois, J., Skene, N.G., Hansen, T.F., Kogelman, L.J.A., Watson, H.J., Liu, Z., Eating Disorders Working Group of the Psychiatric Genomics Consortium, International Headache Genetics Consortium, 23andMe Research Team, Brueggeman, L., et al. (2020). Genetic identification of cell types underlying brain complex traits yields insights into the etiology of Parkinson's disease. *Nat. Genet.* 52, 482–493. <https://doi.org/10.1038/s41588-020-0610-9>.
16. Agarwal, D., Sandor, C., Volpatto, V., Caffrey, T.M., Monzón-Sandoval, J., Bowden, R., Alegre-Abarrategui, J., Wade-Martins, R., and Webber, C. (2020). A single-cell atlas of the human substantia nigra reveals cell-specific pathways associated with neurological disorders. *Nat. Commun.* 11, 4183. <https://doi.org/10.1038/s41467-020-17876-0>.
17. Leinartaitė, L., and Svensson, P. (2017). Folding Underlies Bidirectional Role of GPR37/Pael-R in Parkinson Disease. *Trends Pharmacol. Sci.* 38, 749–760. <https://doi.org/10.1016/j.tips.2017.05.006>.
18. Imai, Y., Soda, M., Inoue, H., Hattori, N., Mizuno, Y., and Takahashi, R. (2001). An unfolded putative transmembrane polypeptide, which can lead to endoplasmic reticulum stress, is a substrate of parkin. *Cell* 105, 891–902. [https://doi.org/10.1016/S0092-8674\(01\)00407-X](https://doi.org/10.1016/S0092-8674(01)00407-X).
19. Yang, H.J., Vainshtein, A., Maik-Rachline, G., and Peles, E. (2016). G protein-coupled receptor 37 is a negative regulator of oligodendrocyte differentiation and myelination. *Nat. Commun.* 7, 10884. <https://doi.org/10.1038/ncomms10884>.
20. Qian, Z., Li, H., Yang, H., Yang, Q., Lu, Z., Wang, L., Chen, Y., and Li, X. (2021). Osteocalcin attenuates oligodendrocyte differentiation and myelination via GPR37 signaling in the mouse brain. *Sci. Adv.* 7, eabi5811. <https://doi.org/10.1126/sciadv.abi5811>.
21. Kamath, T., Abdulaouf, A., Burris, S.J., Langlieb, J., Gazestani, V., Nadaf, N.M., Balderrama, K., Vanderburg, C., and Macosko, E.Z. (2022). Single-cell genomic profiling of human dopamine neurons identifies a population that selectively degenerates in Parkinson's disease. *Nat. Neurosci.* 25, 588–595. <https://doi.org/10.1038/s41593-022-01061-1>.
22. Meyer, R.C., Giddens, M.M., Schaefer, S.A., and Hall, R.A. (2013). GPR37 and GPR37L1 are receptors for the neuroprotective and glioprotective factors prosaptide and prosaposin. *Proc. Natl. Acad. Sci. USA* 110, 9529–9534. <https://doi.org/10.1073/pnas.1219004110>.
23. Roesch, K., JadHAV, A.P., Trimarchi, J.M., Stadler, M.B., Roska, B., Sun, B.B., and Cepko, C.L. (2008). The transcriptome of retinal Muller glial cells. *J. Comp. Neurol.* 509, 225–238. <https://doi.org/10.1002/cne.21730>.
24. Huang, H., He, W., Tang, T., and Qiu, M. (2023). Immunological Markers for Central Nervous System Glia. *Neurosci. Bull.* 39, 379–392. <https://doi.org/10.1007/s12264-022-00938-2>.
25. Wong, Y.C., and Krainc, D. (2017). alpha-synuclein toxicity in neurodegeneration: mechanism and therapeutic strategies. *Nat. Med.* 23, 1–13. <https://doi.org/10.1038/nm.4269>.
26. Kim, S., Kwon, S.H., Kam, T.I., Panicker, N., Karuppagounder, S.S., Lee, S., Lee, J.H., Kim, W.R., Kook, M., Foss, C.A., et al. (2019). Transneuronal Propagation of Pathologic alpha-Synuclein from the Gut to the Brain Models Parkinson's Disease. *Neuron* 103, 627–641.e7. <https://doi.org/10.1016/j.neuron.2019.05.035>.
27. Wang, R., Ren, H., Kaznacheeva, E., Lu, X., and Wang, G. (2023). Association of Glial Activation and alpha-Synuclein Pathology in Parkinson's Disease. *Neurosci. Bull.* 39, 479–490. <https://doi.org/10.1007/s12264-022-00957-z>.
28. Qian, H., Kang, X., Hu, J., Zhang, D., Liang, Z., Meng, F., Zhang, X., Xue, Y., Maimon, R., Dowdy, S.F., et al. (2020). Reversing a model of Parkinson's disease with *in situ* converted nigral neurons. *Nature* 582, 550–556. <https://doi.org/10.1038/s41586-020-2388-4>.
29. Piallat, B., Benazzouz, A., and Benabid, A.L. (1996). Subthalamic nucleus lesion in rats prevents dopaminergic nigral neuron degeneration after striatal 6-OHDA injection: behavioural and immunohistochemical studies. *Eur. J. Neurosci.* 8, 1408–1414. <https://doi.org/10.1111/j.1460-9568.1996.tb01603.x>.
30. Mostofi, A., Morgante, F., Edwards, M.J., Brown, P., and Pereira, E.A.C. (2021). Pain in Parkinson's disease and the role of the subthalamic nucleus. *Brain* 144, 1342–1350. <https://doi.org/10.1093/brain/awab001>.
31. Luan, Y., Tang, D., Wu, H., Gu, W., Wu, Y., Cao, J.L., Xiao, C., and Zhou, C. (2020). Reversal of hyperactive subthalamic circuits differentially mitigates pain hypersensitivity phenotypes in parkinsonian mice. *Proc. Natl. Acad. Sci. USA* 117, 10045–10054. <https://doi.org/10.1073/pnas.1916263117>.
32. Ip, C.W., Klaus, L.C., Karikari, A.A., Visanji, N.P., Brotchie, J.M., Lang, A.E., Volkmann, J., and Koprich, J.B. (2017). AAV1/2-induced overexpression of A53T-alpha-synuclein in the substantia nigra results in degeneration of the nigrostriatal system with Lewy-like pathology and motor impairment: a new mouse model for Parkinson's disease. *Acta Neuropathol. Commun.* 5, 11. <https://doi.org/10.1186/s40478-017-0416-x>.
33. Anderson, J.P., Walker, D.E., Goldstein, J.M., de Laat, R., Banducci, K., Caccavello, R.J., Barbour, R., Huang, J., Kling, K., Lee, M., et al. (2006).

- Phosphorylation of Ser-129 is the dominant pathological modification of alpha-synuclein in familial and sporadic Lewy body disease. *J. Biol. Chem.* 281, 29739–29752. <https://doi.org/10.1074/jbc.M600933200>.
34. Fujiwara, H., Hasegawa, M., Dohmae, N., Kawashima, A., Masliah, E., Goldberg, M.S., Shen, J., Takio, K., and Iwatsubo, T. (2002). alpha-Synuclein is phosphorylated in synucleinopathy lesions. *Nat. Cell Biol.* 4, 160–164. <https://doi.org/10.1038/ncb748>.
 35. Savitt, J.M., Jang, S.S., Mu, W., Dawson, V.L., and Dawson, T.M. (2005). Bcl-x is required for proper development of the mouse substantia nigra. *J. Neurosci.* 25, 6721–6728. <https://doi.org/10.1523/JNEUROSCI.0760-05.2005>.
 36. Zeis, T., Enz, L., and Schaeren-Wiemers, N. (2016). The immunomodulatory oligodendrocyte. *Brain Res.* 1641, 139–148. <https://doi.org/10.1016/j.brainres.2015.09.021>.
 37. Ma, X.R., Zhu, X., Xiao, Y., Gu, H.M., Zheng, S.S., Li, L., Wang, F., Dong, Z.J., Wang, D.X., Wu, Y., et al. (2022). Restoring nuclear entry of Sirtuin 2 in oligodendrocyte progenitor cells promotes remyelination during ageing. *Nat. Commun.* 13, 1225. <https://doi.org/10.1038/s41467-022-28844-1>.
 38. Bang, S., Xie, Y.K., Zhang, Z.J., Wang, Z., Xu, Z.Z., and Ji, R.R. (2018). GPR37 regulates macrophage phagocytosis and resolution of inflammatory pain. *J. Clin. Invest.* 128, 3568–3582. <https://doi.org/10.1172/JCI99888>.
 39. Qin, X.Y., Zhang, S.P., Cao, C., Loh, Y.P., and Cheng, Y. (2016). Aberrations in Peripheral Inflammatory Cytokine Levels in Parkinson Disease: A Systematic Review and Meta-analysis. *JAMA Neurol.* 73, 1316–1324. <https://doi.org/10.1001/jamaneurol.2016.2742>.
 40. Mogi, M., Harada, M., Narabayashi, H., Inagaki, H., Minami, M., and Nagatsu, T. (1996). Interleukin (IL)-1 beta, IL-2, IL-4, IL-6 and transforming growth factor-alpha levels are elevated in ventricular cerebrospinal fluid in juvenile parkinsonism and Parkinson's disease. *Neurosci. Lett.* 211, 13–16. [https://doi.org/10.1016/0304-3940\(96\)12706-3](https://doi.org/10.1016/0304-3940(96)12706-3).
 41. Mogi, M., Harada, M., Kondo, T., Riederer, P., Inagaki, H., Minami, M., and Nagatsu, T. (1994). Interleukin-1 beta, interleukin-6, epidermal growth factor and transforming growth factor-alpha are elevated in the brain from parkinsonian patients. *Neurosci. Lett.* 180, 147–150. [https://doi.org/10.1016/0304-3940\(94\)90508-8](https://doi.org/10.1016/0304-3940(94)90508-8).
 42. Sterling, J.K., Kam, T.I., Guttha, S., Park, H., Baumann, B., Mehrabani-Tabari, A.A., Schultz, H., Anderson, B., Alnemri, A., Chou, S.C., et al. (2022). Interleukin-6 triggers toxic neuronal iron sequestration in response to pathological alpha-synuclein. *Cell Rep.* 38, 110358. <https://doi.org/10.1016/j.celrep.2022.110358>.
 43. Tatton, W.G., Chalmers-Redman, R., Brown, D., and Tatton, N. (2003). Apoptosis in Parkinson's disease: signals for neuronal degradation. *Ann. Neurol.* 53, S61–S72, discussion S70–62. <https://doi.org/10.1002/ana.10489>.
 44. Park, H., Kam, T.I., Peng, H., Chou, S.C., Mehrabani-Tabari, A.A., Song, J.J., Yin, X., Karuppagounder, S.S., Umanah, G.K., Rao, A.V.S., et al. (2022). PAAN/MIF nuclease inhibition prevents neurodegeneration in Parkinson's disease. *Cell* 185, 1943–1959.e21. <https://doi.org/10.1016/j.cell.2022.04.020>.
 45. Oliveras-Salva, M., Van der Perren, A., Casadei, N., Stroobants, S., Nuber, S., D'Hooge, R., Van den Haute, C., and Baekelandt, V. (2013). rAAV2/7 vector-mediated overexpression of alpha-synuclein in mouse substantia nigra induces protein aggregation and progressive dose-dependent neurodegeneration. *Mol. Neurodegener.* 8, 44. <https://doi.org/10.1186/1750-1326-8-44>.
 46. Duke, D.C., Moran, L.B., Pearce, R.K.B., and Graeber, M.B. (2007). The medial and lateral substantia nigra in Parkinson's disease: mRNA profiles associated with higher brain tissue vulnerability. *Neurogenetics* 8, 83–94. <https://doi.org/10.1007/s10048-006-0077-6>.
 47. Moran, L.B., Duke, D.C., Deprez, M., Dexter, D.T., Pearce, R.K.B., and Graeber, M.B. (2006). Whole genome expression profiling of the medial and lateral substantia nigra in Parkinson's disease. *Neurogenetics* 7, 1–11. <https://doi.org/10.1007/s10048-005-0020-2>.
 48. Zeng, Z., Su, K., Kyaw, H., and Li, Y. (1997). A novel endothelin receptor type-B-like gene enriched in the brain. *Biochem. Biophys. Res. Commun.* 233, 559–567. <https://doi.org/10.1006/bbrc.1997.6408>.
 49. Donohue, P.J., Shapira, H., Mantey, S.A., Hampton, L.L., Jensen, R.T., and Battey, J.F. (1998). A human gene encodes a putative G protein-coupled receptor highly expressed in the central nervous system. *Brain Res. Mol. Brain Res.* 54, 152–160. [https://doi.org/10.1016/s0169-328x\(97\)00336-7](https://doi.org/10.1016/s0169-328x(97)00336-7).
 50. Marazziti, D., Golini, E., Gallo, A., Lombardi, M.S., Matteoni, R., and Tocchini-Valentini, G.P. (1997). Cloning of GPR37, a gene located on chromosome 7 encoding a putative G-protein-coupled peptide receptor, from a human frontal brain EST library. *Genomics* 45, 68–77. <https://doi.org/10.1006/geno.1997.4900>.
 51. Murakami, T., Shoji, M., Imai, Y., Inoue, H., Kawarabayashi, T., Matsubara, E., Harigaya, Y., Sasaki, A., Takahashi, R., and Abe, K. (2004). Pacl-R is accumulated in Lewy bodies of Parkinson's disease. *Ann. Neurol.* 55, 439–442. <https://doi.org/10.1002/ana.20064>.
 52. Morato, X., Garcia-Esparcia, P., Argerich, J., Llorens, F., Zerr, I., Paslawski, W., Borras, E., Sabido, E., Petaja-Repo, U.E., Fernandez-Duenas, V., et al. (2021). Ecto-GPR37: a potential biomarker for Parkinson's disease. *Transl. Neurodegener.* 10, 8. <https://doi.org/10.1186/s40035-021-00232-7>.
 53. Patarini, R., Rong, Y., Qu, C., and Morgan, J.I. (2008). Distinct mechanisms of 1-methyl-4-phenyl-1,2,3,6-tetrahydropyrimidine resistance revealed by transcriptome mapping in mouse striatum. *Neuroscience* 155, 1174–1194. <https://doi.org/10.1016/j.neuroscience.2008.06.064>.
 54. Marazziti, D., Golini, E., Mandillo, S., Magrelli, A., Witke, W., Matteoni, R., and Tocchini-Valentini, G.P. (2004). Altered dopamine signaling and MPTP resistance in mice lacking the Parkinson's disease-associated GPR37/parkin-associated endothelin-like receptor. *P Natl Acad Sci USA* 101, 10189–10194. <https://doi.org/10.1073/pnas.0403661101>.
 55. Liu, B., Mosienko, V., Vaccari Cardoso, B., Prokudina, D., Huettelmann, M., Teschemacher, A.G., and Kasparov, S. (2018). Glio- and neuro-protection by prosaposin is mediated by orphan G-protein coupled receptors GPR37L1 and GPR37. *Glia* 66, 2414–2426. <https://doi.org/10.1002/glia.23480>.
 56. Meyer, R.C., Giddens, M.M., Coleman, B.M., and Hall, R.A. (2014). The protective role of prosaposin and its receptors in the nervous system. *Brain Res.* 1585, 1–12. <https://doi.org/10.1016/j.brainres.2014.08.022>.
 57. Chen, Y.P., Gu, X.J., Ou, R.W., Zhang, L.Y., Hou, Y.B., Liu, K.C., Cao, B., Wei, Q.Q., Song, W., Zhao, B., et al. (2021). Genetic Analysis of Prosaposin, the Lysosomal Storage Disorder Gene in Parkinson's Disease. *Mol. Neurobiol.* 58, 1583–1592. <https://doi.org/10.1007/s12035-020-02218-4>.
 58. Oji, Y., Hatano, T., Ueno, S.I., Funayama, M., Ishikawa, K.I., Okuzumi, A., Noda, S., Sato, S., Satake, W., Toda, T., et al. (2020). Variants in saposin D domain of prosaposin gene linked to Parkinson's disease. *Brain* 143, 1190–1205. <https://doi.org/10.1093/brain/awaa064>.
 59. Tayebi, N., Lopez, G., Do, J., and Sidransky, E. (2020). Pro-cathepsin D, Prosaposin, and Progranulin: Lysosomal Networks in Parkinsonism. *Trends Mol. Med.* 26, 913–923. <https://doi.org/10.1016/j.molmed.2020.07.004>.
 60. Hiraiwa, M., Martin, B.M., Kishimoto, Y., Conner, G.E., Tsuji, S., and O'Brien, J.S. (1997). Lysosomal proteolysis of prosaposin, the precursor of saposins (sphingolipid activator proteins): its mechanism and inhibition by ganglioside. *Arch. Biochem. Biophys.* 341, 17–24. <https://doi.org/10.1006/abbi.1997.9958>.
 61. Tian, R., Abarrientos, A., Hong, J., Hashemi, S.H., Yan, R., Dräger, N., Leng, K., Nalls, M.A., Singleton, A.B., Xu, K., et al. (2021). Genome-wide CRISPRi/a screens in human neurons link lysosomal failure to ferroptosis. *Nat. Neurosci.* 24, 1020–1034. <https://doi.org/10.1038/s41593-021-00862-0>.
 62. Lin, Z.H., Ruan, Y., Xue, N.J., Fang, Y., Pu, J.L., and Zhang, B.R. (2021). PSAP intronic variants around saposin D domain and Parkinson's disease. *Brain* 144, e3. <https://doi.org/10.1093/brain/awaa354>.

63. Lefrancois, S., May, T., Knight, C., Bourbeau, D., and Morales, C.R. (2002). The lysosomal transport of prosaposin requires the conditional interaction of its highly conserved d domain with sphingomyelin. *J. Biol. Chem.* 277, 17188–17199. <https://doi.org/10.1074/jbc.M200343200>.
64. He, Y., Kaya, I., Shariatgorji, R., Lundkvist, J., Wahlberg, L.U., Nilsson, A., Mamula, D., Kehr, J., Zareba-Paslawska, J., Biverstål, H., et al. (2023). Prosaposin maintains lipid homeostasis in dopamine neurons and counteracts experimental parkinsonism in rodents. *Nat. Commun.* 14, 5804. <https://doi.org/10.1038/s41467-023-41539-5>.
65. Azevedo, C., Teku, G., Pomeshchik, Y., Reyes, J.F., Chumariana, M., Russ, K., Savchenko, E., Hammarberg, A., Lamas, N.J., Collin, A., et al. (2022). Parkinson's disease and multiple system atrophy patient iPSC-derived oligodendrocytes exhibit alpha-synuclein-induced changes in maturation and immune reactive properties. *Proc. Natl. Acad. Sci. USA* 119, e2111405119. <https://doi.org/10.1073/pnas.2111405119>.
66. Rose-John, S., Jenkins, B.J., Garbers, C., Moll, J.M., and Scheller, J. (2023). Targeting IL-6 trans-signalling: past, present and future prospects. *Nat. Rev. Immunol.* 23, 666–681. <https://doi.org/10.1038/s41577-023-00856-y>.
67. Lacroix, M., Rousseau, F., Guilhot, F., Malinge, P., Magistrelli, G., Herren, S., Jones, S.A., Jones, G.W., Scheller, J., Lissila, R., et al. (2015). Novel Insights into Interleukin 6 (IL-6) Cis- and Trans-signaling Pathways by Differentially Manipulating the Assembly of the IL-6 Signaling Complex. *J. Biol. Chem.* 290, 26943–26953. <https://doi.org/10.1074/jbc.M115.682138>.
68. Rose-John, S., and Heinrich, P.C. (1994). Soluble receptors for cytokines and growth factors: generation and biological function. *Biochem. J.* 300, 281–290. <https://doi.org/10.1042/bj3000281>.
69. Hunter, C.A., and Jones, S.A. (2015). IL-6 as a keystone cytokine in health and disease. *Nat. Immunol.* 16, 448–457. <https://doi.org/10.1038/ni.3153>.
70. Zhang, Y., Chen, K., Sloan, S.A., Bennett, M.L., Scholze, A.R., O'Keeffe, S., Phatnani, H.P., Guarneri, P., Caneda, C., Ruderisch, N., et al. (2014). An RNA-sequencing transcriptome and splicing database of glia, neurons, and vascular cells of the cerebral cortex. *J. Neurosci.* 34, 11929–11947. <https://doi.org/10.1523/JNEUROSCI.1860-14.2014>.
71. Yun, S.P., Kam, T.I., Panicker, N., Kim, S., Oh, Y., Park, J.S., Kwon, S.H., Park, Y.J., Karuppagounder, S.S., Park, H., et al. (2018). Block of A1 astrocyte conversion by microglia is neuroprotective in models of Parkinson's disease. *Nat. Med.* 24, 931–938. <https://doi.org/10.1038/s41591-018-0051-5>.
72. Liberatore, G.T., Jackson-Lewis, V., Vukosavic, S., Mandir, A.S., Vila, M., McAuliffe, W.G., Dawson, V.L., Dawson, T.M., and Przedborski, S. (1999). Inducible nitric oxide synthase stimulates dopaminergic neurodegeneration in the MPTP model of Parkinson disease. *Nat. Med.* 5, 1403–1409. <https://doi.org/10.1038/70978>.
73. Ma, Q., Cao, Z., Yu, Y., Yan, L., Zhang, W., Shi, Y., Zhou, N., and Huang, H. (2017). Bombyx neuropeptide G protein-coupled receptor A7 is the third cognate receptor for short neuropeptide F from silkworm. *J. Biol. Chem.* 292, 20599–20612. <https://doi.org/10.1074/jbc.M117.815191>.
74. Dixon, W.J. (1980). Efficient analysis of experimental observations. *Annu. Rev. Pharmacol. Toxicol.* 20, 441–462. <https://doi.org/10.1146/annurev.pa.20.040180.002301>.
75. Xie, Y.K., Luo, H., Zhang, S.X., Chen, X.Y., Guo, R., Qiu, X.Y., Liu, S., Wu, H., Chen, W.B., Zhen, X.H., et al. (2022). GPR177 in A-fiber sensory neurons drives diabetic neuropathic pain via WNT-mediated TRPV1 activation. *Sci. Transl. Med.* 14, eabh2557. <https://doi.org/10.1126/scitranslmed.abh2557>.
76. Hao, Y., Hao, S., Andersen-Nissen, E., Mauck, W.M., 3rd, Zheng, S., Butler, A., Lee, M.J., Wilk, A.J., Darby, C., Zager, M., et al. (2021). Integrated analysis of multimodal single-cell data. *Cell* 184, 3573–3587.e29. <https://doi.org/10.1016/j.cell.2021.04.048>.

STAR★METHODS

KEY RESOURCES TABLE

REAGENT or RESOURCE	SOURCE	IDENTIFIER
Antibodies		
Rabbit anti-TH	Millipore	Cat# AB152; RRID:AB_390204
Sheep anti-TH	Novus Biologicals	Cat# NB300-110; RRID:AB_10002491
Rat anti-NeuN	Asis Biofarm	Cat# OB-PRT013-01
Mouse anti-APC	Sigma-Aldrich	Cat# OP80; RRID:AB_2057371
Goat anti-Iba1	Novus Biologicals	Cat# NB100-1028; RRID:AB_3148646
Mouse anti-GFAP	Millipore	Cat# MAB360; RRID:AB_11212597
Chicken anti-β-Gal	Abcam	Cat# ab9361; RRID:AB_307210
Rabbit anti-olig2	Sigma-Aldrich	Cat# MABN50; RRID:AB_10807410
Rabbit anti-ATF3	Novus Biologicals	Cat# NBP1-85816; RRID:AB_11014863
Rabbit anti-α-synuclein	Abcam	Cat# ab138501; RRID:AB_2537217
Rabbit Anti-PSAP	Proteintech	Cat# 10801-1-AP; RRID:AB_2172462
Mouse anti-β-actin	Sigma-Aldrich	Cat# MAB1501; RRID:AB_2223041
Sheep anti-Prealbumin (TTR)	Abcam	Cat# ab9015; RRID:AB_306943
Rabbit anti-Phospho-p44/42 MAPK (pERK1/2)	Cell Signaling Technology	Cat# 4370s; RRID:AB_2315112
Rabbit anti-ERK1/ERK2 (tERK1/2)	ABclonal	Cat# A16686; RRID:AB_2770274
DAPI	Vector laboratories	Cat# H-1200; RRID:AB_2336790
Donkey anti-mouse IgG H&L-488	Abcam	Cat# ab150105; RRID:AB_2732856
Donkey anti-mouse IgG H&L-Cy3	Jackson	Cat# 715-165-150; RRID:AB_2340813
Donkey anti-mouse IgG H&L-Cy5	Jackson	Cat# 715-175-150; RRID:AB_2340819
Donkey anti-rabbit IgG H&L-488	Abcam	Cat# ab150073; RRID:AB_2636877
Donkey anti-rabbit IgG H&L-Cy3	Jackson	Cat# 711-165-152; RRID:AB_2307443
Donkey anti-rabbit IgG H&L-647	Abcam	Cat# ab150075; RRID:AB_2752244
Donkey anti-goat IgG H&L-488	Abcam	Cat# ab150129; RRID:AB_2687506
Donkey anti-goat IgG H&L-Cy3	Abcam	Cat# ab6949; RRID:AB_955018
Donkey anti-goat IgG H&L- Cy5	Jackson	Cat# 705-175-147; RRID:AB_2340415
Donkey anti-chicken IgG H&L-Cy3	Jackson	Cat# 703-165-155; RRID:AB_2340363
Donkey anti-chicken IgG H&L- Cy5	Jackson	Cat# 703-175-155; RRID:AB_2340365
Donkey anti-sheep IgG H&L-488	Abcam	Cat# ab150177; RRID:AB_2801320
HRP-rabbit anti-sheep IgG	Earthox	Cat# E030150
HRP-goat anti-rabbit IgG	Earthox	Cat# E030120; RRID:AB_3073916
HRP-goat anti-mouse IgG	Earthox	Cat# E030110; RRID:AB_2572419
Bacterial and virus strains		
AAV9-SYN-SNCA (A53T)-EGFP-3×FLAG-WPRE	Obio Technology	Cat# H8638
AAV9-hSyn-EGFP-3×FLAG-WPRE	Obio Technology	Cat# AOV062
AAV8-pDIO-DSE-mCherry-PSE-shIL-6	Vector Core at ZJU	N/A
AAV9-CAG-mCherry-T2A-Cre	Obio Technology	Cat# H2893
Chemicals, peptides, and recombinant proteins		
Prosaposin-derived 14-mer peptide (TX-14)	QYAOBIO	N/A
Recombinant IL-6 Protein	R&D Systems	Cat# 406-ML
6-hydroxydopamine (6-OHDA)	Tocris	Cat# 2547
Apomorphine Hydrochloride (APO)	U.S. Pharmacopeia	Cat# R08440
DMEM/F12	Gibco	Cat# 11320082
poly-D-lysine	Sigma-Aldrich	Cat# P0899
Neurobasal medium	Gibco	Cat# 21103049

(Continued on next page)

Continued

REAGENT or RESOURCE	SOURCE	IDENTIFIER
B27	Gibco	Cat# 17504044
N2	Gibco	Cat# 17502001
T3	Sigma-Aldrich	Cat# T6397
Tamoxifen	Sigma-Aldrich	Cat# T5648
Critical commercial assays		
Human IL-6 ELISA kits	R&D Systems	Cat# HS600C
Mouse IL-6 ELISA kits	R&D Systems	Cat# M6000B
RNAscope multiplex fluorescent manual assay kit	ACDBio	Cat# 323100
Deposited data		
snRNA-seq dataset of postmortem SNpc	Kamath et al. ²¹	GEO: GSE178265
Transcriptomic expression profile of the SNpc	Moran et al. ⁴⁷	GEO: GSE8397
Experimental models: Cell lines		
HEK293T	ATCC	CRL-3216; RRID: CVCL_0063
Experimental models: Organisms/strains		
<i>Gpr37</i> ^{-/-} mice	Jackson laboratory	Stock #: 005806
<i>Gpr37</i> ^{fl/fl} mice	Cyagen Biosciences	N/A
<i>Psap</i> ^{fl/fl} mice	GemPharmatech	N/A
<i>Plp1-Cre/ER</i> mice	Jackson laboratory	Stock #: 005975
Ai14 (RCL-tdT)-D mice	Jackson laboratory	Stock #: 007914
TH Cre mice	Jackson laboratory	Stock #: 008601
A53T α -synuclein transgenic mice	Jackson laboratory	Stock #: 004479
Oligonucleotides		
See Table S1 for target sequences against mouse IL-6	This paper	
See Table S1 for qRT-PCR primer sequences	This paper	
See Table S1 for primers of GPR37 plasmid cloning	This paper	
Recombinant DNA		
pCMV-Flag-Gpr37	This paper	N/A
pDIO-DSE-mCherry-PSE-MCS	http://n2t.net/addgene:129669	RRID: Addgene_129669
Software and algorithms		
ImageJ/Fiji (NIH)	ImageJ.net	RRID:SCR_003070
GraphPad Prism	Graphpad Software, Inc	RRID:SCR_002798
Other		
RNAscope Probe-Mm-Gpr37	ACDBio	Cat# 319291
RNAscope Probe-Hs-GPR37	ACDBio	Cat# 513631
RNAscope Probe-Mm-Plp1	ACDBio	Cat# 428181
RNAscope Probe-Hs-PLP1	ACDBio	Cat# 564571
RNAscope Probe-Mm-Psap	ACDBio	Cat# 545241
RNAscope Probe-Hs-PSAP	ACDBio	Cat# 583601
RNAscope Probe-Mm-IL-6R	ACDBio	Cat# 438931
RNAscope Probe-Mm-gp130	ACDBio	Cat# 476211
Talos L120C 120 kV transmission electron microscope	Thermo Scientific	
Nikon Eclipse Ni-E microscope	Nikon	
Olympus FluoView FV1000 confocal microscopy	Olympus	

EXPERIMENTAL MODEL AND STUDY PARTICIPANT DETAILS

Animals

The transgenic mouse strains were obtained from the Jackson laboratory and bred in the animal facility of Zhejiang University. *Gpr37*^{fl/fl} mice were generated by Cyagen Biosciences and *Psap*^{fl/fl} mice were generated by GemPharmatech Co., Ltd. *Gpr37* conditional knockout mice were generated by *Plp1-Cre/ER* crossing with *Gpr37*^{fl/fl} mice. *Psap*^{fl/fl} mice were mated with *TH-Cre* mice to obtain *Psap* conditional knockout mice and control littermates. All animals were group-housed at a 12 h light-dark cycle (light on from 8 a.m. to 8 p.m.) with food and water available *ad libitum*. Adult male mice (8–12 weeks) were used for behavioral and pharmacological experiments. Animals were randomly assigned to different experimental groups. Sample sizes were estimated based on our previous experience from similar studies and were sufficient for statistical analyses. All experiments were performed following the National Institutes of Health Guide for the Care and the International Association for the Study of Pain and approved by the Animal Care and Use Committee of Zhejiang University.

Cell cultures

The human embryonic kidney cell line (HEK293T, RRID: CVCL_0063) was maintained in DMEM (Gibco, #11965092) containing 10% FBS, 100 units/mL penicillin, 100 µg/mL streptomycin, and 4 mM L-glutamine at 37°C in a humidified atmosphere containing 5% CO₂.

Primary culture of mouse OPCs was performed as described previously with slight modifications.³⁷ Four newborn mice cerebral cortices were dissected into ice-cold HBSS (Gibco, #14025092) and rinsed with HBSS for three times. After mechanical trituration, the cell suspension was transferred into a T75 flask pre-coated with poly-D-lysine (Sigma-Aldrich, #P0899, 0.1 mg/mL). The cells were maintained in DMEM/F12 (Gibco, #11320082) supplemented with 20% FBS at 37°C with 5% CO₂. The cells were cultured for up to 8 days and the medium was changed every 3 days. The flask was shaken at 200 rpm for 2 h and replaced with fresh medium followed by shaking at 250 rpm for an additional 16 h at 37°C. The cell suspension was centrifuged at 200 g for 5 min and the cells were subcultured in pre-coated dishes for 3–4 h at 37°C with 5% CO₂. The medium was changed to Neurobasal (Gibco, #21103049) medium supplemented with B27 supplement (Gibco, #17504044) and N2 supplement (Gibco, #17502001). The differentiation of OPC into OLs was induced by T3 (Sigma-Aldrich, #T6397, 40 ng/mL) and CNTF (PeproTech, #450-13, 10 ng/mL). To collect oligodendrocyte conditioned medium, the medium was changed to Opti-MEM with either vehicle or TX-14 and cultured for 12 h.

Primary microglial culture was performed as described previously with slight modifications.⁷¹ Whole brains from mouse pups at postnatal day 1 (P1) were obtained. After removal of the meninges, the brains were minced into small pieces (approximate 1 mm²). The brains were transferred to DMEM/F12 supplemented with 8 U/mL papain and 125 U/mL DNase and incubated for 20 min at 37°C in a humidified atmosphere containing 5% CO₂. DMEM/F12 complete medium was used to stop the trypsinization. The brains were washed three times in this medium again. Cell debris and clumps were removed by passing the cell suspension through a 70 µm cell strainer. After centrifuging the cells at 200 g for 10 min at room temperature, the cells were resuspended and seeded in a T75 flask and culture in the humidified incubator (5% CO₂, 37°C), with a complete medium change on day 4. The conditioned medium from the primary oligodendrocyte treat with vehicle or TX-14 were applied to primary cultured microglia for 18 h. The culture media and cell lysate were collected for further analysis.

Human postmortem substantia nigra sections and CSF samples

Human postmortem substantia nigra sections were obtained from donors through the National Health and Disease Human Brain Tissue Resource Center with permission from the Medical Ethics Committee of Zhejiang University School of Medicine. Details regarding the human subjects, including age, gender, and sample size, can be found in the supplemental Table S2. Human samples were allocated to Control and PD groups based on the diagnosis. For human CSF collection, the study was approved by the Ethics Committee of Zhejiang Provincial People's Hospital. The CSF collection was a voluntary CSF donation by the patients and patients consented to their CSF being used for research purpose in anonymized way. The written informed consent was received from participants prior to inclusion in the study. Fresh frozen sections and CSF were immediately stored at –80°C until required. SNpc brain sections and human CSF were utilized for immunofluorescence and immunoblotting, respectively, as described in subsequent sections.

METHOD DETAILS**Viral vectors**

AAV9-SYN-SNCA (A53T)-EGFP-3×FLAG-WPRE (AAV- α Syn), AAV9-hSyn-EGFP-3×FLAG-WPRE (AAV-GFP), and AAV9-CAG-mCherry-T2A-Cre (AAV-Cre-mCherry) were generated and packaged by Obio Technology (Shanghai) Co., Ltd. AAV8-pDIO-DSE-mCherry-PSE-shIL-6 were generated and packaged by the Vector Core at the Zhejiang University, and pDIO-DSE-mCherry-PSE-MCS was a gift from Beatriz Rico (Addgene plasmid #129669, <http://n2t.net/addgene:129669>, RRID: Addgene_129669). The target sequences (listed in Table S1) against mouse *IL-6* were inserted into the *AvrII* and *EcoRI* sites. The viral titers exceeding 10¹² vector genome (vg) mL⁻¹ were used.

Stereotaxic surgery

For unilateral 6-OHDA lesioning, adult mice (8–12 weeks) were anesthetized and then mounted in a stereotaxic instrument (RWD Life Science Co., Ltd). Half an hour before 6-OHDA administration, mice were intraperitoneal injected with 25 mg/kg desipramine and 5 mg/kg pargyline. 1 μ L 6-OHDA (1 μ g/ μ L dissolved in 0.02% ascorbic acid, Tocris, #2547) was unilateral injected into medial forebrain bundle (MFB) according to the following stereotaxic coordinates (relative to bregma): anterior-posterior (A/P) = −1.2 mm, medio-lateral (M/L) = −1.2 mm and dorsoventral (D/V) = −4.75 mm. Sham mice were injected the same value of vehicle (0.9% saline and 0.02% ascorbic acid) into MFB. The injection was applied with a 10 μ L Hamilton syringe and a 36-gauge needle at the rate of 0.1 μ L/min. The needle was remained in place for an additional 5 min before removed. After injection, mice were cleaned and sutured the wound and remained on a heat-pad until completely recovered from anesthesia.

For stereotaxic AAV- α Syn injection, mice were unilaterally injected AAV-GFP or AAV- α Syn into the substantia nigra (A/P = −3.1 mm, M/L = −1.2 mm, and D/V = −4.3 mm). The infusion was performed at a rate of 0.1 μ L/min and 1 μ L of AAV- α Syn or AAV-GFP was injected into the mouse. For the rescue experiment, mice received intraperitoneal injections of tamoxifen (100 mg/kg, daily) for 6 days after 3 weeks of AAV- α Syn administration. Behavioral tests were performed 2 months after injection and mice were euthanized for pharmacological analysis.

For knockdown of *Psap*, AAV-Cre-mCherry was injected into the substantia nigra of *Psap*^{fl/fl} mice according to the following stereotaxic coordinates (2 injections of 0.25 μ L each): A/P = −3.08 mm, M/L = −1.5 mm, D/V = −4.08 mm and A/P = −3.52 mm, M/L = −1.0 mm, D/V = −4.3 mm. For knockdown of *Il-6*, *Plp1-Cre/ER* mice were received two stereotaxic injections of AAV-pDIO-shIL-6 with the same coordinates after 21 days of tamoxifen intraperitoneal injection. WT mice were administrated with equal volume of appropriate virus as controls. Injections were made using the same syringe and needle, at a rate of 0.05 μ L/min. After 3 weeks, 1 μ L of 6-OHDA (1 μ g/ μ L) was injected into ipsilateral MFB and behavioral tests were performed 1 week after injection.

For microinjection of recombinant IL-6 protein and TX-14, a single stainless-steel guide cannula (0.41 mm in diameter, RWD Life Science Co., Ltd, #62004) was implanted into the substantia nigra (A/P = −3.0 mm, M/L = −1.2 mm, and D/V = −4.5 mm). The guide cannula was stabilized to the skull using 2 anchor screws and dental cement. During microinjection, mice were anesthetized with brief 5% isoflurane induction and kept at 1% isoflurane. 0.5 μ L IL-6 (100 ng/ μ L, R&D Systems, #406-ML) was infused using a microinjection cannula for 12 consecutive days. The injection was performed at a rate of 0.1 μ L/min and the microinjection cannula was held in place for an additional 5 min before removed. The control mice were injected with equal volume of saline. For TX-14 injection, 0.5 μ L TX-14 (1 μ g/ μ L, QYAOBIO) was infused using a microinjection cannula for 12 consecutive days. Behavioral tests were performed in next day of the last IL-6 treatment and mice were euthanized for pharmacological analysis.

Immunofluorescence

For staining fixed frozen tissue sections, mice were transcardially perfused with PBS followed by 4% PFA. Whole brains were extracted and post-fixed in 4% PFA overnight at 4°C, and then transferred to 30% sucrose for cryoprotection. Immunofluorescence was performed on 30 μ m thick brain sections. For staining, the slides were blocked with 2% BSA and 0.3% Triton X-100 in PBS at room temperature for 1 h and then incubated with primary antibody at 4°C overnight. After washing three times with PBS, the brain sections were incubated with appropriate fluorescence conjugated secondary antibody for 2 h at room temperature. When antigen retrieval was required, slides were incubated with sodium citrate buffer for 20 min at 95°C before staining. Images were examined and recorded with a CCD SPOT camera (SPOT Imaging). For high-resolution images, sections were also captured under Olympus Fluoview FV1000. The antibodies were used at the following dilutions: chicken anti- β -Gal (1:5000), goat anti-Iba1 (1:1000), mouse anti-GFAP (1:1000), mouse anti-APC (1:200), mouse anti-olig2 (1:200), rabbit anti-ATF3 (1:200), sheep anti-TH (1:1000), and rabbit anti-TH (1:1000) primary antibodies, FITC, cyanine3 (Cy3)- or cyanine5 (Cy5)-conjugated secondary antibodies (1:500, Jackson ImmunoResearch). The total number of TH⁺ dopaminergic neurons were calculated by the stereological method as previously described.⁷² For analyzing fluorescence intensity, at least three coronal sections were selected from each brain, and three mice were measured in each group. The fluorescence intensity was analyzed using NIH ImageJ software.

For staining paraffin-embedded human sections, slides were baked in a dry air oven for 1 h at 65°C and transferred to xylene three times for 10 min each. Then slides were placed in gradient alcohol (100%, 100%, 95%, 85%, 75%) for 5 min respectively. After wash three times with PBS, antigen retrieval and fluorescent staining were performed.

In situ hybridization

The *in situ* hybridization was performed according to the manufacturer's instructions of the RNAscope multiplex fluorescent manual assay kit (Advanced Cell Diagnostics). The brains were prepared in RNase-free condition and 10 μ m thick sections were used for *in situ* hybridization. Prehybridization, hybridization, and washing were performed according to the manufacturer's instructions.

Plasmid construction and transfection

The entire coding region of the *Gpr37* gene (GenBank: NM_010338) was cloned by PCR. The primers used for the PCR cloning see Table S1. The obtained PCR products were inserted into the *HindIII* and *KpnI* sites of the pCMV-Flag vector and the pEGFP-N1 vector for expression in mammalian cells. All the constructs described above were sequenced by Hangzhou Tsingke Biology Co. to verify the sequences and orientations. The GPR37 plasmid construct was transfected into HEK293T cells using Lipofectamine 2000

reagent (Invitrogen) according to the manufacturer's instructions. The cells were used for the following experiments 48–72 h after transfection.

Quantitative real-time PCR

Quantitative real-time PCR was performed as described previously with slight modifications.⁷³ Fresh tissues were dissected under a binocular microscope and total RNA was then extracted using RNeasy Plus Mini kit (Qiagen) in RNase-free conditions. For primary cultured oligodendrocytes, cells were stimulated with TX-14 for 2 h and then homogenized according to the manufacturer's instructions. When required, the cells were treated with various inhibitors prior to initiation of the experiment. The total RNA (0.2 µg) was converted to cDNA using a PrimeScript first strand cDNA synthesis kit (TaKaRa). Gene-specific mRNA abundance was quantified using CFX96 Real-Time RT-PCR system (Bio-Rad). The primer sequences used are listed in Table S1.

Assessment of protein secretion

Cultured medium from treated cells was collected and cell debris was removed by centrifugation. The protein in medium was concentrated by Amicon ultra-0.5 centrifugal filter devices according to manufacturer's protocol. The protein samples were subjected to western blot or ELISA analysis.

Western Blot

The tissues were homogenized in RIPA lysis buffer with protease and phosphatase inhibitors at 4°C for 30 min. Protein concentration were quantified using Pierce BCA Protein Assay Kit. 20 µg of proteins were size-fractionated by SDS-PAGE (10%) and then transferred to a PVDF membrane. The membranes were blocked in TBS containing 0.05% Tween 20 and 5% nonfat dry milk for 1 h at room temperature and then incubated with primary antibody and appropriate horseradish peroxidase-conjugated secondary antibody. For loading control, the blots were probed with actin antibody (1:10,000). The bands were visualized with ECL substrate by Azure Bio-systems. All immunoblots were quantified using NIH ImageJ software.

For ERK1/2 phosphorylation assay, HEK293T cells transiently expressing GPR37 were seeded in 24-well plates and starved for 1 h in serum-free medium to reduce background ERK1/2 activation. After stimulation with the indicated ligand for 5 min, the cells were lysed in 10 µL RIPA lysis buffer at 4°C for 30 min on a rocker and then scraped. If required, the cells were pretreated with PTX for 10–16 h prior to stimulation. Equal amounts of total cell lysate were size-fractionated using SDS-PAGE (10%). The rabbit monoclonal anti-phospho-ERK1/2 (Thr202/Tyr204, 1:1000) and anti-rabbit horseradish peroxidase-conjugated secondary antibody (1:10000) were used according to the manufacturer's protocols. The blots were stripped and relabeled using an anti-total ERK1/2 (1:1000) monoclonal antibody as a control for protein loading. The levels of ERK1/2 phosphorylation were normalized to total ERK1/2.

For human and mouse CSF analysis, samples were diluted with PBS (1:1) and equal volumes of each sample (10 µL) were loaded onto 10% polyacrylamide gels. The remaining steps were performed as with tissues samples. The CSF marker transthyretin (TTR) was detected as loading control and the levels of PSAP secretion were normalized to TTR.

ELISA

Human and mouse IL-6 ELISA kits were performed accounting to manufacturer's protocol. Human and mouse CSF samples and culture media were used to ELISA assay. The standard curve was included in each experiment.

Behavioral scheme

Adult male mice were habituated to the environment for at least 2 days before the testing commenced. All behavioral tests were blindly preformed.

For rotarod test, a rotarod system (IITC Life Science Inc.) was used to assess motor function. Before initiation of the experiment, all animals were trained on rotarod at speed of 6 rpm for two consecutive days. During the tests, the speed of rotation was accelerated from 4 to 40 rpm over a 300 s period. Each mouse was subjected to three trials at least 20 min intervals and the falling latency and speed were recorded.

For open field test, the test was initiated by placing the mouse at the center of a novel open field arena (40 cm length x 40 cm width x 30 cm height) under normal light conditions. The distance was determined during 30 min under Open Field Video Tracking System.

For apomorphine-induced rotation test, apomorphine-induced rotations in mice were performed after 14 days of 6-OHDA induced lesion. Mice were recorded after subcutaneous injection of apomorphine (U.S. Pharmacopeia, #R08440, 1 mg kg⁻¹) using a live video system.

For von Frey test, mice were habituated for 2 h in chambers placed on the elevates metal mesh floor and their hind paws (central surface) were stimulated by a series of von Frey hairs with logarithmically increasing stiffness (0.02–2.56 g, Stoelting). The paw withdrawal thresholds were determined by Dixon's up-down method.⁷⁴

For tail-immersion test, a water bath was used to evaluate the thermal sensitivity with water temperature at 48, 50 or 52°C. The tail (one-third of the length) of mouse was immersed in water and the latency of tail withdrawal was recorded as a nociceptive response.⁷⁵ Each mouse was subjected to three trials at least 1 min intervals.

For pole test, the test was conducted on a 9 mm diameter, 75 cm height vertical pole with bandage gauze. Before the actual test, the mice were trained for two consecutive days and each training session consisted of three test trials. Mice were placed facing up on the top of the pole and the total time to descend the base of the pole were recorded.

Transmission electron microscopy

Transmission electron microscopy was performed as described previously with slight modifications.³⁷ Mice were anaesthetised with sodium pentobarbital (50 mg/kg) and transcardially perfused with 4% glutaraldehyde in 0.1 M phosphate buffer (pH 7.4). The brain was harvested and immersed in 4% glutaraldehyde at 4°C for at least 1 week. Then the region of corpus callosum (CC) and caudate putamen (CPu) were dissected (1 mm³) and immersed into 4% glutaraldehyde at 4°C overnight. The samples were first washed with 0.1 M Cacodylic Acid Sodium (CAS) buffer for 10 min at 4°C for three times and post-fixed in 2% osmium-tetroxide (OsO₄) containing 3% potassium hexacyanoferrate trihydrate (K₃Fe(CN)₆) for 1 h on ice. Then the samples were washed with deionised water for 5 min at 4°C for four times and incubated in 4% aqueous uranyl acetate for 1 h on ice, and then washed with deionised water for 5 min at RT for four times. Next, the samples were dehydrated in 50%, 70%, 90% and 95% acetone for 15 min and 100% acetone for 30 min (10 min per time), respectively. Then the samples were infiltrated in grades of acetate: Epon embedding mixture (1:3, 1:1, 3:1, each for 2 h) and then embedded in a pure Epon mixture overnight. For polymerisation, the samples were embedded in pure Epon at 45°C for 12 h and then transferred to 65°C for 48–72 h. 60 nm ultrathin sections were cut, and double stained with uranyl acetate and lead citrate. Image acquisition was performed with a Thermo Scientific Talos L120C 120 kV transmission electron microscope. Axon diameter and myelin thickness were calculated from a measured area based on assumption of circularity using ImageJ.

Clustering cell into subtypes

Data were collected from GEO: GSE178265.²¹ Only patients of Parkinson and healthy person were kept for further analysis. To minimize the impact of other diseases due to advanced age, samples of patients aged 60 to 80 were retained. The snRNA-seq data were normalized and scaled before cell clustering. Lower expressed genes were filtered out which expressed in less than 10 cells. The effect of percent of ribosome and percent of mitochondrion were regressed out when scaling gene expression. To remove potential batch effect, we used canonical correlation analysis (CCA) and RunUMAP function implemented in Seurat (v4.0)⁷⁶ to reduce dimensionality. Cell clusters were identified using the “FindClusters” function in Seurat. Cells were annotated with classical markers. The natural-log transformed normalized expression data were used to represent genes’ expression level.

QUANTIFICATION AND STATISTICAL ANALYSIS

Statistical analyses

All data were statistically analyzed with GraphPad Prism 6.1 software. Data were presented as means ± SEM. Differences in two set comparisons were analyzed using two-tailed Student’s unpaired *t* test. For more than 2 groups, a one-way ANOVA followed by Bonferroni’s post hoc test was used to assess the statistical significance. For multiple mixed comparisons, a two-way ANOVA followed by Bonferroni’s post hoc test was used. Slopes of G-Ratio versus axon diameter were comparison using simple linear regression analysis. The criteria for statistical differences was: ns (not significant), *p* > 0.05, **p* < 0.05, ***p* < 0.01, ****p* < 0.001, *****p* < 0.0001; and all of the statistical details of experiments can be found in the figure legends. Data presented in figures were statistically assessed as indicated:

Figure 1F: two-tailed Student’s unpaired *t* test.

Figure 1G: two-way ANOVA followed by Bonferroni’s post hoc test.

Figure 2B, D-F, J-M, Q, and S: one-way ANOVA followed by Bonferroni’s post hoc test.

Figure 2G, H, N and O: two-way ANOVA followed by Bonferroni’s post hoc test.

Figure 3B, E-G, and K-N: two-tailed Student’s unpaired *t* test.

Figure 3H, I, O and P: two-way ANOVA followed by Bonferroni’s post hoc test.

Figure 4A, D-F, H, I, L, M, and X (Right): one-way ANOVA followed by Bonferroni’s post hoc test.

Figure 4B, G and T: two-way ANOVA followed by Bonferroni’s post hoc test.

Figure 4K, O-Q, S, U-X (left) and Y: two-tailed Student’s unpaired *t* test.

Figure 5C-E, I, and J: one-way ANOVA followed by Bonferroni’s post hoc test.

Figure 5F and G: two-way ANOVA followed by Bonferroni’s post hoc test.

Figure 6E, G-I, and K: two-tailed Student’s unpaired *t* test.

Figure S1A, two-way ANOVA followed by Bonferroni’s post hoc test.

Figure S2C-E, I-K, M, and O: two-tailed Student’s unpaired *t* test.

Figure S2F and P: two-way ANOVA followed by Bonferroni’s post hoc test.

Figure S2L and N: simple linear regression analysis of slopes.

Figure S3B, D-F (Left), H-J, and O-R (Left): two-tailed Student’s unpaired *t* test.

Figure S3F (Right), K, L and R (Right): two-way ANOVA followed by Bonferroni's post hoc test.

Figure S4A, C, E, G, and K-M: two-way ANOVA followed by Bonferroni's post hoc test.

Figure S4F: one-way ANOVA followed by Bonferroni's post hoc test.

Figure S4I and J: two-tailed Student's unpaired *t* test.

Figure S5B, D, F, and H: one-way ANOVA followed by Bonferroni's post hoc test.

Figure S6C-E: two-tailed Student's unpaired *t* test.